

Pepper, D.W. and D.B. Carrington 2005. *Indoor Air Pollution Modeling*. Chapter 14 of *AIR QUALITY MODELING - Theories, Methodologies, Computational Techniques, and Available Databases and Software. Vol. II – Advanced Topics* (P. Zannetti, Editor). Published by The EnviroComp Institute (<http://www.envirocomp.org/>) and the Air & Waste Management Association (<http://www.awma.org/>).

Chapter 14

Indoor Air Pollution Modeling

Darrell W. Pepper ⁽¹⁾ and David B. Carrington ⁽²⁾

⁽¹⁾ Nevada Center for Advanced Computational Methods, University of Nevada Las Vegas, Las Vegas, Nevada (USA)

darrell.pepper@nscee.edu

⁽²⁾ Computer and Computational Sciences Division, Los Alamos National Laboratory, Los Alamos, New Mexico (USA)

dcarring@lanl.gov

Abstract: Indoor Air Pollution is a major concern to today's engineers, architects, and building occupants. More recent, stringent fire and smoke control ordinances, and concern for building occupants' health, have generated the need to understand the sources of indoor air pollution and predict indoor transport. Heating, ventilation, and air conditioning systems which try to maximize energy efficiency and maintain occupants' comfort and well-being, extensive use of man-made building materials, safety, health and recently encountered security risks have brought the idea of modeling indoor air pollution into the mainstay of building design and operation. Theories of air pollution modeling are presented below. Applicable source terms for indoor air pollution, from the simpler to the complex modeling techniques, are discussed here.

Key Words: indoor air quality, air-conditioning, second-hand smoke, ventilation, building contamination, building safety, numerical modeling, fluid dynamics, turbulence modeling, particulate transport, and resuspension.

Nomenclature

c_p	Specific heat at constant pressure
C_j	Concentration of the j^{th} species
$D_j; D_{jj}$	Fickian diffusivity of the j^{th} species
D	Deterministic forcing function

f_i	Body force in the i^{th} direction
g	Gravitational acceleration
g_{x_i}	Gravitational acceleration in the i^{th} coordinate direction
k	Thermal conductivity
κ	Von Karman constant of proportionality
$K_1 K_2 K_3$	Diagonal components of dispersion tensor in direction of principal axes
K_m	Turbulent exchange coefficient for momentum
L	Reference length
P	Pressure
Pr	Prandtl number
Q	Volumetric source term
q	Heat flux per unit area
$Q_{c,j}$	Concentration source for the j^{th} species
Q_s	Volumetric species source term
\dot{S}	Derivative of species or mass with respect to time
Sc	Schmidt number
T_{hot}	Reference temperature (hot or cold as indicated)
u_i	Velocity in i^{th} direction or i^{th} component
u'	Instantaneous value of fluctuation component of velocity in the x direction
u_*	Friction velocity
u_n	Initial guess or current time velocity
u^{n+1}	Velocity at next time step
u^n	Current or initial velocity
U_i	Velocity vector having components u, v, w
\hat{U}_i	Advection velocity
U_{f_i}	Diffusion velocity
v^*	Predicted velocity
v_{s_j}	Species settling velocity
x_i	i^{th} coordinate direction
$\overline{w'u'}$	Component of turbulent stress tensor

Greek Letter Symbols for Variables and Constants

κ	wave number
μ	Dynamic viscosity
ρ	Density
ρ_{fluid}	Fluid density

σ_{ij}	Stress tensor
ν	Kinematic viscosity
τ	Turbulent flux

Other Mathematical Notation

C^T	Vector transpose of gradient operators
K_{ij}	Dispersion tensor
$L()$	Linear operator L
\mathbf{n}	Vector normal to boundary surface
n_r	Normally distributed random number
Ω	Domain omega
$P_{x_i}(x_i, t)$	Probability distribution function for a three-dimensional space
σ	Standard deviation of a probability distribution
$\sigma(x(t))$	Standard deviation of a probability distribution
σ^2	Covariance of a probability distribution
Γ	Boundary of considered domain
W_i	Polynomial weighting function
$dW(t)$	Wiener process
$\{ \}$	Column vector
$[]$	Row vector or matrix
$\left\{ \begin{matrix} \bullet \\ \mathbf{v} \end{matrix} \right\}$	Time dependent vector of velocity variable
$[\mathbf{A}(\mathbf{u})]$	Advection Matrix
$[\mathbf{K}_v]$	Stiffness Matrix for velocity
$[\mathbf{K}_T]$	Stiffness Matrix for temperature
$[\mathbf{K}_C]$	Stiffness Matrix for concentration
$\{\mathbf{F}_v\}$	Load vector for velocity
$\{\mathbf{F}_T\}$	Load vector for temperature
$\{\mathbf{F}_C\}$	Load vector for concentration
$[\mathbf{M}]$	Mass matrix
N_k	Shape function

Mathematical Operators

$\bar{\mathbf{u}} \bullet \mathbf{n}$	Vector normal dot product
δ_{ij}	Kroneker delta
∇_x	Curl

$\nabla \bullet \vec{u}$	Vector dot product
Δ	First difference
$\frac{D}{Dt}$	Material derivative
$\frac{\partial}{\partial t}$	Time derivative
∇	Gradient operator

1 Introduction

Emission of pollutants and their accumulation due to poor ventilation and air exchange are serious problems that are currently under investigation by many researchers. Of particular concern are issues involving air quality within buildings. Toxic fumes and airborne diseases are known to produce undesirable odors, eye and nose irritations, sickness, and occasionally death. Other products such as tobacco smoke and carbon monoxide can also have serious health effects on people exposed to a poorly ventilated environment; studies indicate that indirect or passive smoking can also lead to lung cancer. Recommendations on outdoor airflow rates to dilute indoor polluted air vary considerably. Due to the demand for large air flow requirements, air quality is usually estimated during the design stage of a ventilation system.

1.1 General Ventilation Systems

Ventilation systems are designed to either prevent contaminants from entering a room or remove contaminants from interior sources within the room. Since ventilation systems are integral to the study of indoor air pollution, it is prudent to at least identify them. A ventilation system consists of several key components:

- (1) the contaminant source
- (2) an exhaust hood
- (3) an air mover
- (4) ducts and fittings
- (5) makeup air
- (6) exhaust air
- (7) a pollutant removal device
- (8) a discharge stack
- (9) air recirculation

Variations of these components are typically found in most ventilation systems designed to deal with indoor air quality and pollutant removal. Figure 1 shows a schematic of a general ventilation system.

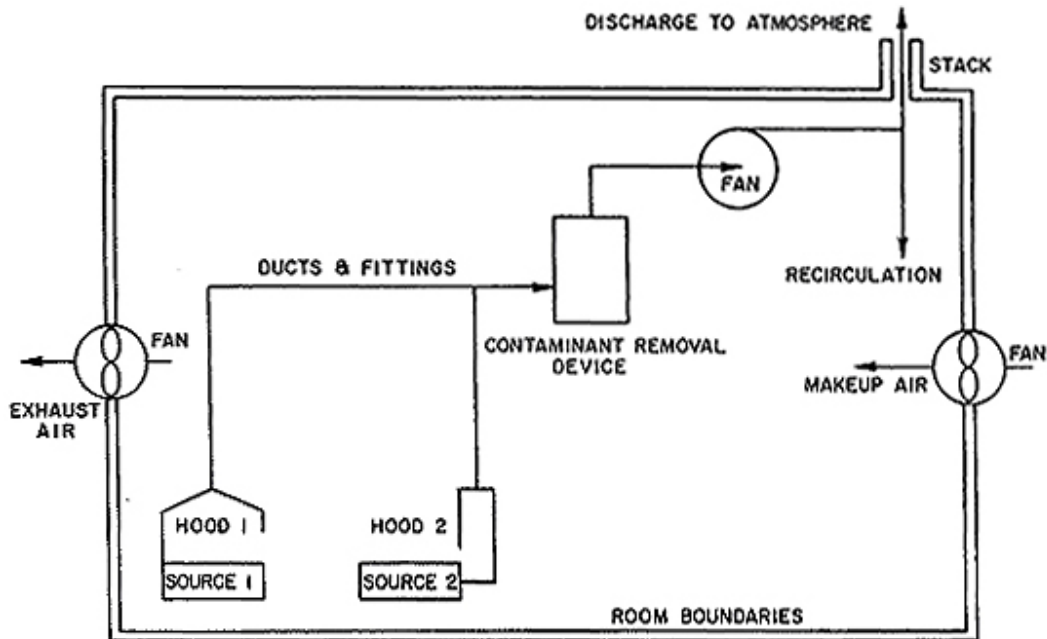


Figure 1. Schematic of a typical ventilation system (from *Industrial Ventilation*, R. J. Heinsohn, J. Wiley & Sons, New York, 1991, pg. 24).

- (1) the contaminant source typically consists of particulates, gases, and vapors generated by various activities
- (2) an exhaust hood is used to contain contaminants emitted from a source (e.g., hoods are used to cover grills in kitchens)
- (3) an air mover, or fan, is used to draw air into a hood
- (4) ducts and fittings make up the piping network connecting the hood to the fan
- (5) makeup air is air that is brought into the room from the outside – this air is usually temperature and humidity controlled
- (6) exhaust air is the air discharged from the room
- (7) a pollutant removal device is a specific piece of equipment used to remove excess contaminant from the room when environmental standards are exceeded
- (8) a discharge stack is a stack that exhausts air into the atmosphere
- (9) air recirculation is air that is returned into the room (clean air)

These components are fairly common in rooms containing ventilation systems, especially industrial settings that deal with dirty environments. More detail describing these components and their proper selection can be found in the ASHRAE Handbook (1981).

1.2 Exposure Risks

The assessment of risk, attributed to exposure to hazardous materials, is a formal field of study. A great deal of effort was spent in developing risk limits during the

early years of the nuclear industry (i.e., in the design and operation of nuclear reactors). A significant amount of mathematical development and theory exists on the subject (Brain and Beck, 1985).

Assessing risk requires information dealing with the types and amounts of material being used and the percent discharged to the environment. Before an accurate risk assessment can be made, it is essential that one have a good grasp of the materials and processes being undertaken. For example, there are over 56,000 manufactured or imported substances used in industrial operations (defined by the EPA in response to the Toxic Substances Control Act). The National Institute for Occupational Safety and Health (NIOSH) also lists a registry of toxic effects of chemical substances (RTECS). Likewise, the Occupational Safety and Health Administration (OSHA) maintains a list of toxic and hazardous materials. These registries are updated every few years and can be obtained from respective agency web sites.

Risk is generally depicted in terms of events per year (usually a small number) and uncertainty (%). Exposure limits are usually depicted in parts per million or billion (denoted as ppm or ppb, or mg/m^3). For example, the risk of getting cancer due to smoking cigarettes (1 pack/day) is 3.6×10^{-3} (annual risk) or a factor of 3 (order of magnitude) in percentage. The permissible exposure limit for acetone, for example, is 750 ppm; respirable dust from marble is $5 \text{ mg}/\text{m}^3$. Table 1 shows a list of some common materials and their permissible exposure limits.

Table 1. Permissible Exposure Limits of Several Materials and Activities.

<i>Material or Activity</i>	<i>Annual Event</i>	<i>%</i>	<i>ppm</i>	<i>mg/m³</i>
Smoking	3.6×10^{-3}	10^{-3}		
chloroform in drinking water	6×10^{-7}	10^{-7}		
Acetone			750	
Chlorine			0.5	
Fluorine			0.1	
Ozone			0.1	
mercury vapor				0.05
marble dust (respirable)				5
grain dust (oat, wheat, barley)				10
wood dust				5

While one can envision various techniques to establish risk, there is a simple technique to obtain a human exposure dose (Ames et al., 1987). This Human Exposure Dose index is related to the Rodent Potency Dose, or HERP, and relates the carcinogenicity of certain chemical agents to animal cancer tests. While one cannot use animal cancer tests to exactly predict human risk, the index does provide a good guide for establishing priorities and potential carcinogenic hazards. The HERP is defined as

$$\text{HERP} = \text{daily lifetime human dose (mg / kg)} \times \text{rodent TD}_{50} \text{ (mg / kg)}$$

where TD_{50} are values taken from a database for 975 chemicals (Ames et al., 1987). Table 2 lists several HERP values.

Table 2. Risk Based on HERP Index (from Ames et al., 1987).

<i>Daily Human Exposure</i>	<i>Dose ($\mu\text{g}/70\text{-kg person}$)</i>	<i>HERP (%)</i>
Chlorinated tap water	Chloroform	0.001
Swimming pool	Chloroform	0.008
Conventional home	Formaldehyde	0.6
Mobile home air	Formaldehyde	2.1
Beer (12 oz)	Ethyl alcohol	2.8
High exposure farm worker	Ethylene dibromide	140.0

1.3 Indoor Air Flow Modeling

In recent years there has been extensive activity in the development and use of Computational Fluid Dynamics (CFD) software and special programs for room air movement and contaminant transport applications. These investigations range from the prediction of air jet diffusion, air velocity and temperature distribution in rooms, spread of contamination in enclosures, to fire and smoke spread inside buildings. In most cases, the predicted results have been promising when compared to available experimental data. However, numerical modeling of ventilation problems is still at an early stage of development. A considerable amount of research and development work is still needed, particularly in the areas of computational schemes, irregular grids, turbulence modeling and wall functions, before CFD can replace physical modeling as a design tool.

One of the earliest attempts to numerically simulate airflow in rooms was conducted by Nielsen (1974) using the stream function-vorticity approach for the dependent variables, along with a two-equation ($k\text{-}\epsilon$) model for turbulence based on the numerical procedure developed by Gosman et al. (1969). The computations produced realistic room flows, but was limited to 2-D. Numerous papers have appeared over the years utilizing the stream function-vorticity approach for simulating 2-D flows within enclosures; however, the approach is *practically* limited to 2-D flows, and does not permit one to easily incorporate turbulence and 3-D effects inherent in actual ventilated enclosures. Efforts were later undertaken by Hjertager and Magnussen (1977), using the finite volume approach and the SIMPLE algorithm developed by Patankar and Spalding (1972), to solve the 3-D primitive equations of motion with the $k\text{-}\epsilon$ two-equation model for turbulence. They modeled the flow from an air jet exhausting into a rectangular room with two ceiling exits. While the point of jet separation from the ceiling was well predicted, the predicted velocity of the jet near the lower region of the room was higher than the measured value.

Gosman et al. (1980) extended their two-dimensional finite volume model to solve isothermal flows within 3-D enclosures with small ventilation openings.

They achieved good correlations of velocity profiles and jet velocity decay with measurements. Sakamoto and Matsuo (1980) similarly predicted 3-D isothermal flow in a room using the marker and cell (MAC) technique (Harlow and Welch, 1965) and two turbulence models: the k- ϵ approach and the large-eddy simulation (LES) technique (Deardorff, 1970). Results compared favorably with measured velocity profiles; they recommended that the k- ϵ approach for turbulence be used for room flow predictions over the LES model because it is simpler to use and requires less computing time for comparable accuracy. A computer program called CAFE, developed by Moulton and Dean (1980), was used to solve the 3-D velocity components, temperature, concentration, and k- ϵ turbulence parameters for flow in industrial enclosures and clean rooms. Results were in good agreement with measurements in regions where velocities were large.

Murakami et al. (1987) investigated the three-dimensional airflow and contamination dispersion in six (rectangular) types of ceiling supply clean rooms both numerically and experimentally for isothermal flow. They used the MAC method coupled with a central difference approach for the velocity components, and a second-order upwind scheme for k, ϵ , and concentration, to solve the transient transport equations. Results showed good agreement between prediction and measurement, as well as some interesting flow phenomena regarding the spread of a jet exhaust as it reached the floor. Awbi (1989) numerically solved 2-D air flow and temperature distributions within rooms with diffusers and various vent locations in an effort to simulate 3-D effects; the 2-D non-isothermal predictions compared well to the measured vertical velocity and temperature profiles in the room. A comprehensive historical discussion and descriptions of numerical methods for solving 2-D and 3-D ventilation and contaminant transport are given by Awbi (1991).

2 Fluid Flow Fundamentals

2.1 Governing Equations

The partial differential equations that describe the flow of fluid, heat, and concentration are all based on the conservation of mass, momentum, thermal energy, and species concentration. The dependent variables are the velocity components, temperature, concentration, and some turbulence variables to account for turbulent flow. These governing equations can be written as

Conservation of Mass

$$\frac{\partial \rho}{\partial t} + \frac{\partial \rho u}{\partial x} + \frac{\partial \rho v}{\partial y} + \frac{\partial \rho w}{\partial z} = 0 \quad (1)$$

Conservation of Momentum: x-direction

$$\rho\left(\frac{\partial u}{\partial t} + u\frac{\partial u}{\partial x} + v\frac{\partial u}{\partial y} + w\frac{\partial u}{\partial z}\right) = -\frac{\partial p}{\partial x} + \frac{\partial \sigma_{xx}}{\partial x} + \frac{\partial \sigma_{xy}}{\partial y} + \frac{\partial \sigma_{xz}}{\partial z} + f_x \quad (2)$$

Conservation of Momentum: y-direction

$$\rho\left(\frac{\partial v}{\partial t} + u\frac{\partial v}{\partial x} + v\frac{\partial v}{\partial y} + w\frac{\partial v}{\partial z}\right) = -\frac{\partial p}{\partial y} + \frac{\partial \sigma_{yx}}{\partial x} + \frac{\partial \sigma_{yy}}{\partial y} + \frac{\partial \sigma_{yz}}{\partial z} + f_y \quad (3)$$

Conservation of Momentum: z-direction

$$\rho\left(\frac{\partial w}{\partial t} + u\frac{\partial w}{\partial x} + v\frac{\partial w}{\partial y} + w\frac{\partial w}{\partial z}\right) = -\frac{\partial p}{\partial z} + \frac{\partial \sigma_{zx}}{\partial x} + \frac{\partial \sigma_{zy}}{\partial y} + \frac{\partial \sigma_{zz}}{\partial z} + f_z \quad (4)$$

Conservation of Energy

$$\rho c_p \left(\frac{\partial T}{\partial t} + u\frac{\partial T}{\partial x} + v\frac{\partial T}{\partial y} + w\frac{\partial T}{\partial z}\right) = \frac{\partial q_x}{\partial x} + \frac{\partial q_y}{\partial y} + \frac{\partial q_z}{\partial z} + Q \quad (5)$$

Species Concentration

$$\frac{\partial C}{\partial t} + u\frac{\partial C}{\partial x} + v\frac{\partial C}{\partial y} + w\frac{\partial C}{\partial z} = \frac{\partial}{\partial x}(D_{xx}\frac{\partial C}{\partial x}) + \frac{\partial}{\partial y}(D_{yy}\frac{\partial C}{\partial y}) + \frac{\partial}{\partial z}(D_{zz}\frac{\partial C}{\partial z}) + S \quad (6)$$

where ρ is density, u , v , and w are horizontal, lateral and vertical velocities, respectively, p is pressure, T is temperature, $f_{x,y,z}$ are velocity body force terms, Q and S are source/sink terms, and D_{xx} , D_{yy} , and D_{zz} are the species concentration diffusion coefficients. The normal and tangential viscous stress terms are defined as:

$$\begin{aligned} \sigma_{xx} &= \frac{2\mu}{3}\left(2\frac{\partial u}{\partial x} + \frac{\partial v}{\partial y} + \frac{\partial w}{\partial z}\right) & \sigma_{yy} &= \frac{2\mu}{3}\left(2\frac{\partial v}{\partial y} + \frac{\partial u}{\partial x} + \frac{\partial w}{\partial z}\right) \\ \sigma_{zz} &= \frac{2\mu}{3}\left(2\frac{\partial w}{\partial z} + \frac{\partial u}{\partial x} + \frac{\partial v}{\partial y}\right) & \sigma_{xy} = \sigma_{yx} &= \mu\left(\frac{\partial u}{\partial y} + \frac{\partial v}{\partial x}\right) \\ \sigma_{xz} = \sigma_{zx} &= \mu\left(\frac{\partial u}{\partial z} + \frac{\partial w}{\partial x}\right) & \sigma_{yz} = \sigma_{zy} &= \mu\left(\frac{\partial v}{\partial z} + \frac{\partial w}{\partial y}\right) \end{aligned} \quad (7)$$

with

$$q_x = \kappa\left(\frac{\partial T}{\partial x}\right) \quad q_y = \kappa\left(\frac{\partial T}{\partial y}\right) \quad q_z = \kappa\left(\frac{\partial T}{\partial z}\right) \quad (8)$$

where μ is dynamic viscosity and κ is thermal conductivity.

2.2 Ideal Fluids

As one can readily see from the complexity of the PDEs described in Equations (1)-(8) for general viscous fluid motion, obtaining solutions to these formidable equations are difficult, generally requiring a numerical approach (CFD). There are instances when one can make simple assumptions regarding overall fluid motion, and the solutions are fairly accurate. These assumptions are based on the premise of the flow being *ideal*, or that the flow is (1) incompressible, (2) inviscid, and (3) irrotational. If the flow under question can be considered ideal, analytical solutions may be used to obtain values for the components of flow, pressure, temperature, and even concentrations.

If the flow is incompressible, the density is constant. This helps in eliminating the effects of compressibility and density variation. An inviscid flow is one in which the viscosity is zero – hence there is no effects attributed to molecular or turbulent diffusion, i.e., no mixing. If these two criteria are valid, then the governing equations reduce to simpler, steady state conditions as shown below:

Conservation of Mass

$$\frac{\partial u}{\partial x} + \frac{\partial v}{\partial y} + \frac{\partial w}{\partial z} = 0 \quad (9)$$

Conservation of Momentum

x-direction

$$u \frac{\partial u}{\partial x} + v \frac{\partial u}{\partial y} + w \frac{\partial u}{\partial z} = -\frac{1}{\rho} \frac{\partial p}{\partial x} \quad (10)$$

y-direction

$$u \frac{\partial v}{\partial x} + v \frac{\partial v}{\partial y} + w \frac{\partial v}{\partial z} = -\frac{1}{\rho} \frac{\partial p}{\partial y} \quad (11)$$

z-direction

$$u \frac{\partial w}{\partial x} + v \frac{\partial w}{\partial y} + w \frac{\partial w}{\partial z} = -\frac{1}{\rho} \frac{\partial p}{\partial z} + g \quad (12)$$

Conservation of Energy

$$\rho c_p \left(u \frac{\partial T}{\partial x} + v \frac{\partial T}{\partial y} + w \frac{\partial T}{\partial z} \right) = \frac{\partial q_x}{\partial x} + \frac{\partial q_y}{\partial y} + \frac{\partial q_z}{\partial z} + Q \quad (13)$$

Species Concentration

$$u \frac{\partial C}{\partial x} + v \frac{\partial C}{\partial y} + w \frac{\partial C}{\partial z} = \frac{\partial}{\partial x} \left(D_{xx} \frac{\partial C}{\partial x} \right) + \frac{\partial}{\partial y} \left(D_{yy} \frac{\partial C}{\partial y} \right) + \frac{\partial}{\partial z} \left(D_{zz} \frac{\partial C}{\partial z} \right) + S \quad (14)$$

A further simplification can be made if the flow is irrotational. Irrotational flow is one in which there is no recirculation or rotation (i.e., the absence of vorticity). This implies a predominance of flow direction with no lateral components. Hence, the velocity components can be grouped into a single value, U , and the momentum equations reduce to Bernoulli's equation

$$\nabla \left(\frac{p}{\rho} + \frac{U^2}{2} + gz \right) = 0 \quad (15)$$

where ∇ is the gradient operator. The quantity $(p/\rho + U^2/2 + gz)$ is constant everywhere, and the flow is irrotational, steady, incompressible, and frictionless (i.e., the flow is *ideal*).

There are numerous solutions to cases involving ideal flow. By introducing the scalar potential functions,

$$u = -\frac{\partial \phi}{\partial x}; \quad v = -\frac{\partial \phi}{\partial y}; \quad w = -\frac{\partial \phi}{\partial z} \quad (16)$$

where ϕ is the scalar potential function. Substituting these expressions into the continuity equation, one obtains the Laplacian:

$$\frac{\partial^2 \phi}{\partial x^2} + \frac{\partial^2 \phi}{\partial y^2} + \frac{\partial^2 \phi}{\partial z^2} = 0 \quad (17)$$

Similarly, a scalar value for the stream function can be introduced for two dimensional flow where

$$u = -\frac{\partial \psi}{\partial y}; \quad v = \frac{\partial \psi}{\partial x} \quad (18)$$

and a Laplacian equation written as

$$\frac{\partial^2 \psi}{\partial x^2} + \frac{\partial^2 \psi}{\partial y^2} = 0 \tag{19}$$

Table 3 lists velocities and derivatives of the potential functions for two-dimensional planar and axisymmetric cylindrical and spherical coordinates.

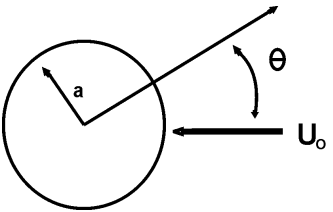
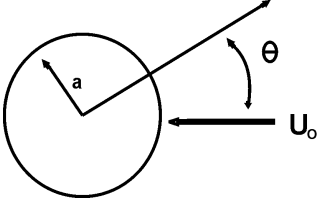
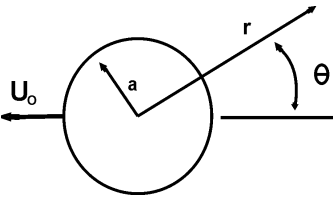
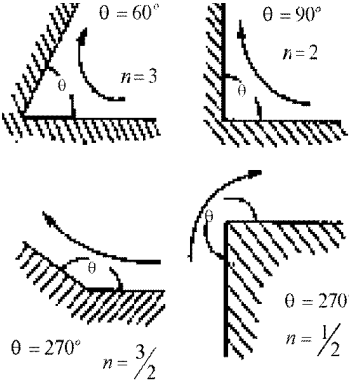
Table 3. Velocities as a Function of ϕ or ψ .

<i>Coordinate System</i>	<i>Velocities - ϕ</i>	<i>Velocities - ψ</i>
2-D Planar	$u = -\frac{\partial \phi}{\partial x}; \quad v = \frac{\partial \phi}{\partial y}$	$u = -\frac{\partial \psi}{\partial y}; \quad v = \frac{\partial \psi}{\partial x}$
2-D Axisymmetric	$u = -\frac{\partial \phi}{\partial r}; \quad v = -\frac{1}{r} \frac{\partial \phi}{\partial \theta}$	$u = -\frac{1}{r} \frac{\partial \psi}{\partial \theta}; \quad v = \frac{\partial \psi}{\partial r}$
3-D Spherical	$u = -\frac{\partial \phi}{\partial r}; \quad v = -\frac{1}{r} \frac{\partial \phi}{\partial \theta}$	$u = -\frac{1}{r^2 \sin \theta} \frac{\partial \psi}{\partial \theta};$ $v = \frac{1}{r \sin \theta} \frac{\partial \psi}{\partial r}$

Utilizing these two variables, potential flow solutions can be obtained for inlets and flanges.

Table 4. Potential Functions for Various Geometries (from *Industrial Ventilation*, R. J. Heinsohn, J. Wiley & Sons, New York, 1991, pg. 374).

Flow	Geometry	Potential relation
Flanged rectangular inlet		$\frac{x}{w} = \cosh\left(\frac{\phi}{k}\right) \cos\left(\frac{\psi}{k}\right)$ $\frac{y}{w} = \sinh\left(\frac{\phi}{k}\right) \sin\left(\frac{\psi}{k}\right); \quad k = q / L\pi$
Unflanged rectangular inlet		$\frac{x}{w} = \frac{1}{\pi} \left[\frac{2\phi}{k} + \exp\left(\frac{2\phi}{k}\right) \cos\left(\frac{2\psi}{k}\right) \right]$ $\frac{y}{w} = \frac{1}{\pi} \left[\frac{2\psi}{k} + \exp\left(\frac{2\phi}{k}\right) \sin\left(\frac{2\psi}{k}\right) \right]$ $k = Q / \pi$
Flanged circular inlet		$\phi = \frac{Q}{2\pi w} \sin^{-1} \left[\frac{2w}{a_1 + a_2} \right]$ $\psi = \frac{Q}{4\pi w} \left[4w^2 - (a_1 - a_2)^2 \right]^{1/2}$ $a_1 = \left[z^2 + (w + r)^2 \right]^{1/2};$ $a_2 = \left[z^2 + (w - r)^2 \right]^{1/2}$

Flow	Geometry	Potential relation
Flow around a stationary cylinder		$\phi = U_0 \cos \theta \left[r + \frac{a^2}{r} \right]$ $\psi = U_0 \sin \theta \left[r - \frac{a^2}{r} \right]$
Flow around a stationary sphere		$\phi = \frac{U_0 \cos \theta}{r^2} \left[r^3 + \frac{a^3}{2} \right]$ $\psi = \frac{U_0 \sin^2 \theta}{2r} \left[r^3 - a^3 \right]$
Flow around a sphere moving in a stationary fluid		$\phi = -\frac{U_0 a^3 \cos \theta}{2r^2}$ $\psi = \frac{U_0 a^3 \sin^2 \theta}{2r}$
Flow in corners		$\phi = -\left(\frac{a}{n}\right) U_w \left(\frac{r}{a}\right)^n \cos(n\theta);$ $U(a, 0) = U(a, \beta) = U_w$ $\psi = -\left(\frac{a}{n}\right) U_w \left(\frac{r}{a}\right)^n \sin(n\theta);$ $n = \pi / \theta$

Analytical solutions to Laplace's equation are harmonic functions (i.e., since the equation is linear and homogeneous, the combination of several solutions to subsets of the problem is also the solution to the overall problem). Hence, a flow field produced by two independent flow fields, each of which can be treated as ideal, can be combined (*superposition principle*) to yield the overall solution. For

example, if ϕ_1 and ϕ_2 are two independent solutions, then the horizontal velocity, u , can be obtained for the entire problem using the relation

$$u = -\frac{\partial\phi}{\partial x} = -\frac{\partial(\phi_1 + \phi_2)}{\partial x} = -\frac{\partial\phi_1}{\partial x} - \frac{\partial\phi_2}{\partial x} = u_1 + u_2 \quad (20)$$

Table 4 lists several potential functions and general cases of flow geometries where analytical solutions can be used to obtain overall values for ϕ and ψ . Several excellent texts that describe the use of potential functions for more complicated flow regimes include Pozrikidis (1999), Woo and Hwang (2000), and the ageless classic by Carslaw and Jaeger (1947).

2.3 Turbulence

A CFD code must be capable of modeling both laminar and turbulent fluid motion. Current approaches to modeling turbulence are based on either "first" or "second-order" closure models in which the governing equations are closed by equations for various turbulence correlation terms (kinetic energy, shear stress, etc.). Examples of such closure schemes are discussed in detail by Jones and Launder (1972). Results show that advanced turbulence closure schemes, incorporating more physics and less empiricism, provide the generality for modeling wider classes of problems and more accurately account for the irregular nature of turbulent flow.

An effective viscosity is usually employed to simplify the solution of the turbulent equations. This concept allows the turbulent stress terms to be conveniently combined with the molecular viscosity (laminar flow) into an overall viscosity term for numerical solution. The two most frequently used approaches to model the effective viscosity (and effective diffusion coefficients) are the Prandtl mixing length model and the k - ϵ two-equation model.

Although the mixing length hypothesis has been successfully applied to solving numerous turbulent flow problems, it has little application in complex flows due to the difficulty in specifying an appropriate length. The method is essentially unsuitable for situations in which recirculation occurs.

In an attempt to more accurately model turbulence within complex regions, especially when recirculation is present, a two-equation turbulence model was first proposed by Jones and Launder (1972). The most common two-equation model is one based on solution of the turbulent kinetic energy, k , and its dissipation rate, ϵ . This model is known as the k - ϵ scheme, and it is popular because of its applicability to a wide range of flow problems (as well as low computational demand over more complex models). The k - ϵ model has been applied to numerous flow problems with good predictive accuracy; also, it is the preferred choice for simulating flows where there is the potential for recirculation and/or swirl.

In the k- ε model, the equation for k (which is derived from the general Navier-Stokes equations) is written as:

$$\begin{aligned} \frac{\partial \rho k}{\partial t} + \frac{\partial \rho u k}{\partial x} + \frac{\partial \rho v k}{\partial y} + \frac{\partial \rho w k}{\partial z} = \\ \frac{\partial}{\partial x} \left(\Gamma_k \frac{\partial k}{\partial x} \right) + \frac{\partial}{\partial y} \left(\Gamma_k \frac{\partial k}{\partial y} \right) + \frac{\partial}{\partial z} \left(\Gamma_k \frac{\partial k}{\partial z} \right) + \mu_\tau \left(2 \left[\left(\frac{\partial u}{\partial x} \right)^2 + \left(\frac{\partial v}{\partial y} \right)^2 + \left(\frac{\partial w}{\partial z} \right)^2 \right] \right. \\ \left. + \left(\frac{\partial u}{\partial y} + \frac{\partial v}{\partial x} \right)^2 + \left(\frac{\partial u}{\partial z} + \frac{\partial w}{\partial x} \right)^2 + \left(\frac{\partial w}{\partial y} + \frac{\partial v}{\partial z} \right)^2 \right) - C_\mu \rho \frac{k^{1.5}}{L} + \beta g \frac{\mu_\tau \partial T}{\sigma_t \partial y} \end{aligned} \quad (21)$$

where $\mu_k = \mu_e / \mu_k$ with $\mu_k \sim 1$, μ_t is the turbulent Prandtl number (0.5 to 0.9) and C_μ is a constant ~ 0.09 . The last term represents the effect of buoyancy.

The transport equation for ε is as follows:

$$\begin{aligned} \frac{\partial \rho \varepsilon}{\partial t} + \frac{\partial \rho u \varepsilon}{\partial x} + \frac{\partial \rho v \varepsilon}{\partial y} + \frac{\partial \rho w \varepsilon}{\partial z} = \\ \frac{\partial}{\partial x} \left(\Gamma_\varepsilon \frac{\partial \varepsilon}{\partial x} \right) + \frac{\partial}{\partial y} \left(\Gamma_\varepsilon \frac{\partial \varepsilon}{\partial y} \right) + \frac{\partial}{\partial z} \left(\Gamma_\varepsilon \frac{\partial \varepsilon}{\partial z} \right) + C_1 \frac{\varepsilon}{k} \mu_\tau \left(2 \left[\left(\frac{\partial u}{\partial x} \right)^2 + \left(\frac{\partial v}{\partial y} \right)^2 \right. \right. \\ \left. \left. + \left(\frac{\partial w}{\partial z} \right)^2 \right] + \left(\frac{\partial u}{\partial y} + \frac{\partial v}{\partial x} \right)^2 + \left(\frac{\partial u}{\partial z} + \frac{\partial w}{\partial x} \right)^2 + \left(\frac{\partial w}{\partial y} + \frac{\partial v}{\partial z} \right)^2 \right) - C_2 \rho \frac{\varepsilon^2}{k} + C_3 \beta g \frac{\varepsilon}{k} \Gamma_t \frac{\partial T}{\partial z} \end{aligned} \quad (22)$$

Here, $\Gamma_t = \mu_e / \mu_\tau$ where μ_τ is a constant equal to 1.22, $C_1 = 1.44$, and $C_2 = 1.92$.

Likewise, the equation for concentration species can be written in similar fashion, i.e.,

$$\begin{aligned} \frac{\partial \rho C}{\partial t} + \frac{\partial \rho u C}{\partial x} + \frac{\partial \rho v C}{\partial y} + \frac{\partial \rho w C}{\partial z} = \frac{\partial}{\partial x} \left(D_{xx} \frac{\partial C}{\partial x} \right) + \frac{\partial}{\partial y} \left(D_{yy} \frac{\partial C}{\partial y} \right) + \frac{\partial}{\partial z} \left(D_{zz} \frac{\partial C}{\partial z} \right) \\ + \frac{\partial}{\partial x} (-\rho u'c') + \frac{\partial}{\partial y} (-\rho v'c') + \frac{\partial}{\partial z} (-\rho w'c') + S \end{aligned} \quad (23)$$

where c' is the deviation from the mean. The terms $-\rho u'c'$, $-\rho v'c'$, and $-\rho w'c'$ are the turbulent diffusion fluxes.

Attempts to simplify the Reynolds stress transport equations are usually made by approximating the advection and diffusion terms into algebraic expressions; such models are referred to as algebraic stress models (ASM). This technique reduces the computational time required to obtain a solution of the transport equations. However, these models have not found wide-scale application in fluid flow problems due to their complexity, and the fact that they still require a large

amount of computing time and do not always produce better predictions than the k - ϵ model.

In large eddy simulation (LES) models, large-scale turbulence fluctuations are solved directly by appropriate transport equations and only the small-scale fluctuations contribute to ϵ . The nonlinear interaction between large-scale and small-scale turbulence motion is approximated through a subgrid-scale turbulent viscosity model. Success of this type of turbulence modeling lies with the computational grid being fine enough to lie within the inertial subrange (Kolmogorov scale) where energy cascade takes place and the dissipation rate, ϵ , has a constant value. The LES method has the ability to freeze the flow at any moment in time; if mean flow quantities are required, the calculations must be conducted over a very long time scale. The application of LES has been relatively limited to isothermal flows in channels and over a cube. However, considerably more work is needed before the method can be applied to a wider range of flow problems.

The accuracy of the solution of the discretized turbulence equations depends on the accuracy of specifying the physical quantities at the boundaries of the flow domain, and on the methods of linking these relations to the bulk flow. Close to a solid boundary, the local Reynolds number is extremely small and turbulent fluctuations are damped out by the proximity of the surface - laminar shear becomes a locally dominant force as a result of the steep velocity gradient. Because of the damping effect of the wall, the transport equations for the turbulence quantities do not apply close to the wall. One way of dealing with this problem is to add extra source terms to the transport equations for k and ϵ , and use an extremely fine grid close to the surface so that the first few points are within the laminar sublayer. This technique is effective, but it requires a vast number of grid points (especially in three-dimensions).

An alternative, and more popular, approach is to use Couette flow analysis and apply algebraic relations (logarithmic laws or wall functions) close to the surface. This approach does not require an ultra-fine grid near the surface. At a point close to the wall, the momentum equation is reduced to a one-dimensional form with gradients in the direction normal to the surface.

Boundary conditions at vent inlets are usually set to fully developed profiles, unless specified directly by the user from experimental data. Likewise, at exits, the transverse velocity components are normally set to zero and the longitudinal exit velocity calculated from mass balance. Exit values for k and ϵ are usually not required because the Reynolds number at the exit is typically large; likewise, the gradients normal to the flow direction of the dependent variables may also be set to zero at the exit plane. A particularly nice feature when using finite element methods is the ability to set the traction terms (i.e., the RHS of the governing equations) equal to zero at the exit. This is the true mathematical formulation for proper specification of the outflow boundary conditions, and does not require a

priori judgment by the user (Gresho et al., 1984) when using finite volume or finite difference schemes.

2.4 Species Transport

It is well known that contamination produced in a ventilated room can quickly spread over the whole zone, especially in a mixing ventilation system with a large rate of entrainment and a circulatory motion created by jets. Normally, the transport equation for concentration is solved either in time-average form or time-dependent form after a converged solution has been achieved for the other transport equations (velocity, temperature, and k - ϵ turbulence parameters). When low concentration levels exist in a room environment (~ 100 ppm), the difference in density between the contaminant and air is usually ignored. This practice is fairly common in both research and industrial applications with regards to either gas or small particulate transport. Nielsen (1981) used this approach to model 2-D concentration distributions within enclosures to investigate the importance of room aspect ratios on concentration distribution; a decrease in height of the room air supply slot produced a decrease in concentration in the enclosure. *Higher room concentrations were found to exist when the contamination source was placed in a relatively stagnant region in the room.* Murakami et al. (1983) obtained similar conclusions from their three-dimensional simulations, and were later confirmed by Davidson (1989) using a 3-D, k - ϵ turbulence model.

The spread of smoke within an L-shaped (rectangular) shopping mall was investigated by Markatos and Cox (1986) using the PHOENICS finite volume code. Both steady-state and transient spread of smoke from a fire was modeled, and results compared with experimental measurements. Agreement between measurement and prediction was generally satisfactory with small differences in the velocity profiles near the top of the doorway openings and in the temperature profiles at the center of the doorways (where cold air entering from the lower region meets the hot smoke leaving the upper region).

Several commercially available CFD codes are being used for simulating room ventilation and contaminant dispersion. The code CFX, developed by AERE Harwell, is a variant of the SIMPLE technique (Patankar, 1980), and resembles the PHOENICS code. This code incorporates finite volumes and unstructured meshes to account for irregular surfaces, and was used to simulate the fire that occurred in Kings Cross Station in London several years ago. Likewise, the FLOVENT code, which is similar to the PHOENICS and CFX, allows one to perform 2-D and small-scale 3-D problems on high performance PCs. Unfortunately, the code does not allow one to handle irregular geometries - curved surfaces must be approximated by orthogonal grids (this effect leads to the stair-step appearance for irregular boundaries and can degrade the ability of a code to accurately resolve boundary layer effects and turbulence near surfaces).

3 Contaminant Sources

Contaminants in buildings generally consist of either particles or gases. Particles can either be in the form of solids or liquids. Gases are generally gaseous or exist as a vapor, both of which obey the perfect gas law. The Glossary of Fundamentals of Industrial Hygiene (1993) gives the following definitions for specific airborne contaminants:

Dusts: Solid particles typically created from crushing, handling, detonation, and impact of organic or inorganic materials; particles do not diffuse in air but settle under the influence of gravity.

Gas: Material state of matter with very low density and viscosity that responds to changes in temperature and pressure; gas diffuses and uniformly distributes itself throughout any enclosure.

Vapors: Gaseous form of substances normally in solid or liquid state at room temperature and pressure; vapors diffuse and mix with the environment – evaporation is the changing of a liquid into a vapor state.

Aerosols: Liquid droplets or solid particles that are dispersed in air with diameters generally in the range of 0.01 - 100 μm ; aerosols generally remain suspended in air for some time.

Fume: Particulate created from the evaporation of solid materials and dispersed into the air; fumes are usually less than 1 μm in diameter.

Mists: Suspended liquid droplets generated from condensation as a gas transforms to a liquid state or by a liquid dispersing into the air due to foaming, splashing, or atomizing; mist forms when a finely divided liquid becomes suspended in air.

Smoke: Particles (suspension of aerosols in air) created from combustion or sublimation, and consists of droplets as well as dry particles, (e.g., tobacco produces a wet smoke composed of tarry droplets); carbon or soot particles are generally less than 0.1 μ in size and result from incomplete combustion of carbon-based materials.

The mass of particles per unit volume of gas is known as the mass concentration (C), often referred to simply as concentration. A variety of units are used for concentration, but the most common is mg/m^3 .

The sources of building contamination and the multitude of contaminants are numerous. Many of the indoor pollution problems stem from construction activities of operations within a facility. Such contaminants include volatile organic compounds (VOCs), pesticides, biological contaminants promoted by moisture, asbestos, radon, lead, and PCBs.

3.1 Building Materials

A major portion of indoor air contaminants come from building materials and equipment. VOCs resulting from the manufacturing and installation processes typically migrate into the air. The majority of VOCs can be classified into the following categories (Hays et al., 1995).

Adhesives, sealants, and architectural coatings: these types of coatings are installed wet and dry or cure on the premises; the solvents used in the formulation of these materials directly relate to the VOCs emitted. The resins used in the base of adhesives are either natural or synthetic, and range from low to high emission rates; sealants consist of putties, caulking compounds, rubber, acrylic latexes, and silicones while architectural coatings include paints, stains, sealers, and varnishes.

Particleboard and plywood: particleboard is a composite produce made from wood chips or residues that are bonded together with adhesives and typically come from milling or woodworking waste. Plywood consists of several thin layers or plies of wood that are bonded by adhesive and are generally classified as either softwood or hardwood; the indoor air quality (IAQ) effects of softwood and hardwood vary with the adhesive (phenol-formaldehyde, PF, and urea-formaldehyde, UF, resins).

Carpet, resilient flooring, and wall covering: these types of materials bring VOC-emitting composition into the building interior along with the use of adhesives to attach the material to various surfaces. Carpets typically consist of fibers of either wool or synthetics. Resilient flooring is generally either tile or sheet (vinyl or rubber). Wall coverings are made from paper, fabric, and vinyl.

Table 5. Partial List of Building Materials and their Emissions (from Hays et al., 1995).

Material	Chemical emitted	Emission rate
Adhesives	Alcohols	
	Amines	
	Benzene	
	Toluene	
Sealants	Alcohols	
	Amines	
	Benzene	
	Xylenes	
Architectural coatings	paints – C4-benzene	
	paints - Toluene	
	stains/varnishes – Amines	
	stains/varnishes - Benzene	
Particleboard	Amines	
	Formaldehyde	0.2-2 mg/m ³ /h
	n-Hexane	15-26 µg/m ³ /h
Carpeting	4-Phenylcyclohexene	0.1 mg/m ³ /h(latex backed)
	Styrene	
Resilient Flooring	Amines	

	Alkanes	
	Linoleum - Trichloroethylene	3.6 $\mu\text{g}/\text{m}^2/\text{h}$
Wall Coverings	Amines	
	Xylenes	
Insulation	foam - Acetone	ND-0.02 $\text{mg}/\text{m}^2/\text{h}$
	Chloroform	ND-0.002 $\text{mg}/\text{m}^2/\text{h}$
Furnishings	Upholstery – Formaldehyde	

Insulation, acoustical ceiling tile, and furnishings: these types of materials include a variety of paints, adhesives, backing, fabrics, and fibrous materials all of which combine to contribute to VOCs. Insulation is commonly thermal oriented, but acoustical and fireproofing also are used; these usually exist in the form of batt and rigid foam consisting of fiberglass or mineral wool. Furnishings include such items as prefabricated movable partitions, workstations, desks, chairs, couches, photocopiers, computers, etc.

Table 5 is a partial list of materials and some of the chemicals emitted from their surfaces, along with emission rates when known. When building materials have a high-surface-area-to-room-volume ratio, it is important to quantify the emissions and their rates to avoid harmful effects to occupants.

3.2 Typical Operations

The most common carriers of pollutants are ventilation systems and the human body (general work activity and socialization). The ventilation system serves as an ideal transport mechanism for dispersing particulates and gaseous compounds throughout a building. Similarly, the human body acts as a repository from transporting all forms of pollutants within a room as well as to other humans.

Operations commonly found in many industrial and office environments include processes such as maintenance and housekeeping, which permit dust or particulate buildup that leads to indoor air contamination. Likewise, office equipment, including such devices as wet and dry copying machines, computers, laser printers, and color inkjet printers emit VOCs during operation. Pest control, construction activities in occupied buildings, moisture leaks, and many industrial activities including chemical spills, grinding, pouring, and sprays lead to indoor contamination. Operations involving food preparation and consumption are particularly sensitive to emissions and unsanitary conditions that lead to indoor air quality problems. Even the natural process of evaporation and diffusion of volatile liquids stored in rooms are common contributors to overall air quality.

3.3 Diffusion in Air

Contamination enters the air by either puff or continuous source emission. A puff is an instantaneous release, or burst, of material of short duration. A continuous emission occurs when a source of pollutant is emitted over a long time, leading to a discernable plume emanating from the source location. The transport physics

attributed to both occurrences obey the conservation of mass, as previously described by Equation (23). Much has been written on the atmospheric dispersion of puffs and plumes of contaminants (Pasquill and Smith, 1985), especially if one can reduce the PDE form of Equation (23) to a more manageable form that can be solved analytically. These analytical solutions are based on the use of Gaussian assumptions (i.e., statistical representations of the probability of concentration being found at specific locations). However, use of such reduced equation sets requires information from the user that may be unknown. This is discussed in more detail in the chapter on Gaussian and analytical solutions. For convenience, we restate the relations here:

Puff:

$$C(x, y, z) = \left(\frac{Q}{(2\pi)^{3/2} \sigma_x(t) \sigma_y(t) \sigma_z(t)} \right) \exp - \left[\frac{(x - Ut)^2}{2\sigma_x^2} + \frac{y^2}{2\sigma_y^2} + \frac{z^2}{2\sigma_z^2} \right] \quad (24)$$

Plume:

$$C(x, y, z) = \left(\frac{Q}{2\pi\sigma_y\sigma_z U} \right) \exp \left(\frac{-y^2}{2\sigma_y^2} \right) \left[\exp \left(\frac{-(z-H)^2}{2\sigma_z^2} \right) + \exp \left(\frac{-(z+H)^2}{2\sigma_z^2} \right) \right] \quad (25)$$

where Q is the source term, U is the principal velocity (or speed) of the air, x, y, z are spatial distances (from either the puff center or the plume source), H is the height of the release, and σ_x , σ_y , and σ_z are the standard deviations, or diffusion coefficients (which are found using empirical relations developed by Pasquill and Gifford – the Pasquill-Gifford curves - see Pasquill and Smith, 1985). Solutions for C from Equations (24)-(25) produce Gaussian probability values which yield circular distributions that can be plotted for specific deviations from the center of the puff or plume – these are usually calculated out to $\pm 3\sigma$ standard deviations.

The diffusion coefficient of particles of diameter D_p can be estimated from the relation (Fuchs, 1964)

$$D = \frac{\kappa TC}{3\pi\mu D_p} \quad (26)$$

$$\sigma = \sqrt{2Dt}$$

where κ is the Boltzmann constant, μ is the molecular viscosity of the carrier gas, C is a constant, D_p is the droplet diameter, t is time, and σ is the standard deviation, or diffusion coefficient. Table 6 shows particle size versus diffusion coefficient in air at STP.

Table 6. Particle Diffusion Coefficients in Air (STP) (from *Industrial Ventilation*, R. J. Heinsohn, J. Wiley & Sons, New York, 1991, pg. 180).

D_p (μm)	D (cm^2/s)
0.01	1.35×10^{-4}
0.05	6.82×10^{-6}
0.10	2.21×10^{-6}
0.50	2.74×10^{-7}
1.00	1.27×10^{-7}
5.00	2.38×10^{-8}
10.00	1.38×10^{-8}

There are numerous book sources that give the molecular diffusion coefficients for a variety of gases. One of the most commonly used source is the CRC Handbook of Physics and Chemistry, which can be found in nearly every library. An equation developed by Chen and Othmer (Vargaftik, 1975) can also be used to obtain the binary gas diffusion coefficient (D_{12} in cm^2/s)

$$D_{12} = \left(\frac{0.43}{K} \right) \left(\frac{T}{100} \right)^{1.81} \sqrt{ \left(\frac{1}{M_1} \right) + \left(\frac{1}{M_2} \right) } \quad (27)$$

$$K = EP \left(\frac{T_{c1} T_{c2}}{10000} \right)^{0.1405}, \quad E = \left[\left(\frac{v_{c1}}{100} \right)^{0.4} + \left(\frac{v_{c2}}{100} \right)^{0.4} \right]^2$$

where v_c and T are the critical volume ($\text{cm}^3/\text{g-mol}$) and temperature ($^\circ\text{K}$), M_1 and M_2 are the molecular weights, and pressure P is in atmospheres. To obtain the diffusion coefficient at temperatures and pressures other than STP,

$$D(P, T) = D(\text{STP}) \left(\frac{1}{P} \right) \left(\frac{T}{298} \right)^{1.81} \quad (28)$$

Table 7 lists some common diffusion coefficients in air for several chemical compounds.

Table 7. Diffusion Coefficients for Several Contaminants in Air (from *Industrial Ventilation*, R. J. Heinsohn, J. Wiley & Sons, New York, 1991, pg. 658).

Substance	M	D ($10^{-5} \text{ m}^2/\text{s}$)
Acetone	56	0.83
Ammonia	17	2.2
Benzene	78	0.77
Chloroform	119	0.87
Hexane	86	0.8
Methane	16	2.2
Sulfur dioxide	64	1.3
Toluene	92	0.71

3.4 Evaporation of Droplets

Drops of liquids are formed from a myriad of industrial and everyday operations. Droplets are basically formed as a result of spraying, aerating, or atomizing. In addition, gas rising through a liquid may ultimately collapse at the liquid's surface and produce liquid droplets. Every drop has a liquid-air interface; it is this interface through which the liquid of the drop, or the liquid contaminant within the drop, evaporates. The physics associated with droplet formation and evaporation are well known, and can be found in detail in various textbooks dealing with cloud physics – a well known reference is the work by Pruppacher and Klett (1978).

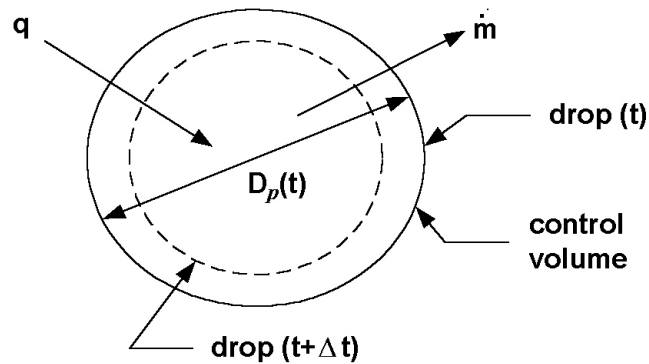


Figure 2. Schematic of an evaporating drop.

The physical processes associated with droplet evaporation can best be illustrated using Figure 2. Vapor escapes from the surface of the drop due to the vapor pressure of the saturated liquid being greater than the partial pressure of the vapor in the far field. The drop diameter, D_p , decreases as the liquid evaporates which in turn affects the rate of evaporation. The evaporating liquid removes energy from the drop and lowers the drop temperature below the ambient air temperature; this process lowers the drop pressure at the drop-air interface. Since evaporation lowers the drop temperature below the air temperature, energy is transferred to the drop by convection from the surrounding air. The mass and heat transfer are strongly coupled and thus control the rate of drop evaporation.

The set of differential equations that describe the evaporation rate, temperature, and diameter of a drop are fairly well established. These three simultaneous differential equations are typically written in the form

$$\begin{aligned} \dot{m} &= C_1 \pi M D_p \left(\frac{D_{ac}}{R_u} \right) Sc^{b_1} Re^{a_1} \left[\left(\frac{P_{r,i}}{T_p} \right) - \left(\frac{P_{v,o}}{T_o} \right) \right] \\ \dot{m} &= - \frac{\rho \pi D_p^2}{2} \frac{dD_p}{dt} \\ \frac{d(T_o - T_p)}{dt} &= - \left(\frac{6h_L}{\rho D_p c_v} \right) (T_o - T_p) + \frac{6mh_{fg}}{\rho \pi D_p^3 c_v} \end{aligned} \quad (29)$$

where Sc is the Schmidt number, Re is the Reynolds number, R_u is the universal gas constant, h_L is the average heat transfer coefficient, c_v is the specific heat at constant volume, and h_{fg} is the enthalpy of vaporization. The equation set in Equation (29) is best solved numerically. If the drop temperature at the liquid-air interface is known, the diameter of the drop can be calculated as a function of time by equating the first two relations. To compute the drop temperature, a simple energy balance as shown in Figure 2 gives the expression for q ,

$$q = \frac{mc_v dT_p}{dt} + u_f \frac{dm}{dt} + \dot{m} h_g(T) \quad \text{where} \quad m = \frac{\rho \pi D_p^3}{6} \quad (30)$$

where u_f is the internal energy of the saturated liquid and h_g is the enthalpy of the saturated vapor. For droplets with diameters less than 100 μm , the heat transfer within the drop is so rapid that the temperature within the drop can be considered to be uniform. For drops larger than 100 μm , the equation set (29) must be solved. The evaporation rate can be calculated from the first relation in Equation (29). Table 8 lists several drop sizes, mass, the mass flow rate (or evaporation rate), and temperature difference between ambient and drop temperatures.

Table 8. Particle diameter, mass, m, and temperature difference (from *Industrial Ventilation*, R. J. Heinsohn, J. Wiley & Sons, New York, 1991, pg. 216).

D_p (μm)	m (kg)	m (kg/s)	$T_o - T_p$ ($^{\circ}\text{C}$)
5	6.54×10^{-14}	1.08×10^{-10}	0.45
10	5.23×10^{-13}	2.16×10^{-10}	0.63
50	6.54×10^{-11}	1.18×10^{-9}	6.58
100	5.23×10^{-10}	2.74×10^{-9}	14.48

For particle sizes less than 10 μm , the particle temperature is essentially the same as the ambient temperature.

3.5 Resuspension of Particulate

Resuspension refers to the entrainment of a particulate into the air stream. The amount that is entrained into the air stream can be estimated using resuspension factors, resuspension rates, and fractional releases. Fractional releases provide an initial amount of contaminant injected into the fluid media.

Resuspension factors are defined as

$$\chi = \frac{C(\text{m}^3)}{C(\text{m}^2)} \quad (31)$$

where the quotient χ is airborne concentration per cubic meter of air divided by the surface concentration per square meter. Resuspension factors are not very useful for estimating quantities of particulate being entrained over time (changing or depleting surface concentration). However, they supply an effective method to evaluate the amount injected into the airflow by an activity at any one time, provided the surface concentration is known. Resuspension rates or mass fractions rates are defined as the fraction of contaminant released over time.

For low flow rates, resuspension coefficients must be specified. Approximations of resuspension rates or factors (mass flux into the domain) are based on the activity occurring and are listed below in this section. For disturbances from turbulent mixing, analytical calculation as developed by Martin et al. (1983) may be sufficient. An injection rate based on empirical evidence is desired.

Particulate entrainment is accomplished when attached particles move. A stream velocity large enough to accomplish this is defined as the threshold speed or threshold friction velocity $u_{*threshold}$. Once particles move, the adhesive forces are much weaker, and the particles are available for entrainment. The forces responsible for breaking the attachment are a function of shear stresses acting on the particle, particulate impingement from already suspended material, and adhesive forces between the surface and the particulate. Martin et al. (1983)

determined resuspension analytically, giving the resuspension rate as a function of friction velocity,

$$u_* = \sqrt{\frac{\tau_{wall}}{\rho_{fluid}}} \quad (32)$$

where τ_{wall} is the shear stress at the wall.

Threshold friction speed is determined from a semi-empirical relation as

$$A = (0.108 + 0.0323/B - 0.00173/B^2)(1 + 0.055/\rho_{fluid} g d_{part}^2)^{1/2} \quad (33)$$

where $A = u_{*threshold} / [(\rho_{part} - \rho_{fluid}) g d_p / \rho_{part}]^{1/2}$ and $B = u_{*threshold} d_{part} \rho_{fluid} / \mu_{fluid}$.

The equation is used for the range $0.22 \leq B \leq 10$.

For $B \leq 0.22$:

$$A = 0.266(1 + 0.055/\rho_{fluid} g d_{part}^2)^{1/2} (1 + 2.123/B)^{-1/2} \quad (34)$$

is used. Since $u_{*threshold}$ appears in both terms of the equality, iteration is required to obtain a solution.

Suspension occurs for particles having physical diameters smaller than $52 \mu\text{m}$ when the threshold velocity is reached. Particle suspension is assumed to occur when the terminal settling velocity, v_s , is equal to the friction velocity and the friction velocity is greater than the threshold velocity.

The amount of material suspended is given by

$$q_s = q_{horizontal} (c_{vert} / u_*^3 c_{hort}) \left[\left(\frac{u_*}{u_{*threshold}} \right)^{\text{Mass\%Suspended}/3} - 1 \right] \quad (35)$$

where: $q_{horizontal} = 2.61 \frac{\rho_{fluid}}{g} (u_* + u_{*threshold})^2 (u_* - u_{*threshold})$

and $c_{vert} = 2 \times 10^{-10}$ and $c_{hort} = 1 \times 10^{-6}$.

There are limitations on the use of this equation since the empirical constants were found by using light soil particles lying on flat thick beds without obstructions to disturb air flow. However, the equation form is proper, only needing experimental results for determining constants.

Threshold velocities for dense substances such as lead are calculated by Martin et al. (1983) to have a minimum value at about 0.3 m/sec for a 49 μm diameter particle. Smaller particles have much greater threshold friction velocities. Determination of the friction velocities on the walls in the laminar sublayer will allow for the incorporation of this resuspension equation provided the species is lying on a thick bed. Application of the above equation to other circumstances will require empirical data.

3.6 Coagulation of Particulate

Another source (and sink for particles) is by coagulation of smaller particles into larger particles as they collide. The time rate of change of concentration from agglomeration for particles with different sizes is given by (Reist, 1993)

$$\frac{dC}{dt} = \frac{-K_o}{2} C^2 \quad (36)$$

where $K_o = K_{12} = 2\pi (d_{part_1} + d_{part_2})(D_1 + D_2)$.

Over a relative short period of time, small particles will coagulate by diffusion into larger particles. For a monodispersed particulate ($D_1 = D_2$) of initial concentration of 1000 / cm^3 , the time for half the particles to coagulate is 55 hours. The time for the particle size to double for this case is 16 days. For an initial concentration of 100,000 / cm^3 , the coagulation half-life is 33 minutes and the size doubling time is 4 hours (Hinds, 1982). The time dependent relationship does not include source and sink terms that would also be affecting equations of concentration.

A deposition velocity by diffusion for particles with a micron aerodynamic diameter is insufficient to remove many of the small particles. However, time for coagulation is of the order of the air exchange rate. Therefore, any small particles would have a propensity to agglomerate to a size large enough for settling velocities to possibly be an effective scavenger. Typically, there will be some concentration of particles in the ambient air referred to as Total Suspended Particulate or TSP.

4 Design Criteria

Design for prevention or remediation of indoor air pollution requires expertise in optimizing geometrical configurations, knowledge of HVAC systems, perceived or expected contaminants and source locations, and economics. Much of the design concept involves ways in which to optimize benefits or balance the advantages and disadvantages of various configurations and equipment. The fact that a room or building will conceivably become contaminated is generally an

accepted fact – to what extent indoor air pollution will become critical is not really known until it happens. Most companies have a somewhat formal design process when developing preliminary designs and concepts – much of this relies on company administrative policies and the experience of the designer. In addition, consultants with specific areas of expertise can play a major role in orchestrating the overall design and configuration of equipment, materials, and potential exposures. In general, the designer must take into account the activities and processes being undertaken in the room or building, the movement of people, and the anticipated costs associated with using the best versus barely acceptable.

4.1 Exposure Levels

There are numerous agencies and organizations that have attempted to establish exposure limits to various chemicals and materials. These standards are typically referred to as threshold limit values (TLV), permissible exposure limits (PEL), and maximum acceptable concentrations (MAC). The American Conference of Governmental and Industrial Hygienists use TLV; the Occupational Safety and Health Administration (OSHA) publishes PEL values; the American National Standards Institute use MAC. While all three are generally compatible, PEL values are backed by law – it is usually prudent for the engineer or scientist to always check with OSHA for the PEL values. Table 9 shows a partial list of substances and the OSHA established PEL.

Table 9. Partial List of OSHA Permissible Exposure Limits.

Substance	PEL* (ppm)
Acetic acid	10
Benzene	10
Chloroform	2
Formaldehyde	3
Ozone	0.1
Turpentine	100

*TWA values

There are several limits that are commonly used in evaluating exposure. The first of these is the time-weighted average of concentration. This is the amount of concentration that workers are exposed to during a normal, 8-hr day, 5 days per week without causing adverse effects.

$$\begin{aligned} \text{TWA}(8\text{ - hr}) &= \left(\frac{1}{8}\right) \int_0^8 c(t) dt \\ \text{TWA}(40\text{ - hr}) &= \left(\frac{1}{40}\right) \int_0^{40} c(t) dt \end{aligned} \quad (37)$$

Short-term exposure limit is the maximum concentration to which workers can be exposed continuously up to 15 minutes without suffering from side effects.

$$\text{STEL} = \left(\frac{1}{15} \right) \int_0^{15} c(t) dt \quad (38)$$

Exposure hazards for a mixture of gaseous contaminants are defined by OSHA using an exposure parameter

$$\text{En} = \sum_i \left(\frac{c}{L} \right)_i \quad (39)$$

where c_i is the measured concentration and L_i is the PEL in comparable units of concentration. If $\text{En} > 1$, exposure is considered to be beyond acceptable limits.

An interesting contaminant that gets greatly overlooked is noise. Longitudinal pressure waves ranging from 20 – 20,000 Hz are known as sound waves. Hearing can be impaired when individuals are exposed to sound or noise above certain amplitudes and lengths of time. Sound power (W) is related to sound intensity by the relation

$$W = (4\pi r^2) \left(\frac{P^2}{\rho a} \right) \quad (40)$$

where a is the speed of sound, ρ is density, r is distance from the source, and P is pressure. Sound intensity (I) is usually used for the expression $(P^2/\rho a)$. A sound-intensity level (L_I) can be defined as

$$L_I = 10 \log_{10} \left(\frac{I}{I_o} \right) \quad (41)$$

where $I_o = 10^{-12} \text{ W/m}^2$ and corresponds to the intensity at reference pressure ($P_o = 2 \times 10^{-5} \text{ N/m}^2$). Sound pressure (L_p) can be calculated at locations from a piece of equipment or process generating noise using the simple formula

$$L_p = L_w - 20 \log_{10} r(m) + 10 \log_{10} Q - 11 \quad (42)$$

where L_w is the sound power and Q is the directivity factor defined as the ratio of the sound power of a small omnidirectional hypothetical source to the sound power of an actual source at the same sound pressure level. The decibel (dB) is the unit used to express sound pressure level, sound intensity level, and sound power.

4.2 Economics

Economics is certainly a factor that must be considered when dealing with issues involving design and remediation of indoor air pollution. The two major costs are Total Capital Cost (TCC) and Total Revenue Requirements (TRR). TCC is essentially the initial costs consisting of money spent to design, build, and install various systems and equipment. TRR are monies spent that must be factored in to the TCC and the revenue needed to provide annual operating costs. Total Indirect Costs (TIC) are monies needed to pay for overhead, i.e., construction expenses, contractors fees, loan interest, building rental, etc. Total Direct Costs (TDC) consists of TCC plus TIC. The TIC is usually a fraction of the TDC. The equation is simply

$$TCC = TDC + TIC = TDC(1 + ICF) \quad (43)$$

where ICF is the Indirect Cost Factor. The TRR is composed of total variable costs (TVC) plus total fixed costs (TFC), or

$$TRR = TVC + TFC \quad (44)$$

Capital recovery cost (CRC) and the fixed cost factor (FCF) are calculated as follows:

$$CRC = TCC \times FCF$$

$$FCF = \frac{[i(1+i)^t]}{[(1+i)^t - 1]} \quad (45)$$

where i is the annual interest rate and t is the capital recovery period (years). Table 10 outlines the various costs and economic factors that should be considered.

Table 10. Cost factors for designing and building ventilation systems (from *Industrial Ventilation*, R. J. Heinsohn, J. Wiley & Sons, New York, 1991, pg. 154).

TCC	
TDC	TIC in % of TDC
Equipment	Construction expense (10-15%)
Labor	Contingencies (5-30%)
Materials	Contractors fees (4-6%)
Structures	Engineering (4-6%)
Consulting fees	Interest during construction (10-25%)
	Start-up costs (10-15%)
	Working capital (2-4%)
	Total ICF (45-100%)
TRR	
TVC	TFC in % of TCC
Administration	Capital recovery cost (11-23%)
Electric, gas, water	Taxes (3-7%)
Maintenance labor	Insurance (1-3%)
Maintenance material	Interim replacement (1-7%)
Operating labor	Tax credits (0-5%)
Supervision	
Raw materials	Total FCF (16-40%)

5 Simple Modeling Techniques

There are generally two concepts used when developing simple models for indoor air quality calculations: (1) well-mixed and (2) partially-mixed ventilation models. In a well-mixed model, the concentration is spatially uniform within the enclosure; in a partially-mixed model, the concentration is nonuniform generally due to poor mixing. In some situations, it is convenient and relatively safe to assume well-mixed conditions – this type of assumption leads to the use of simple analytical models. Unfortunately, most real world situations involve dealing with partially-mixed hypothesis. Analytical procedures are available for these situations as well, but they are somewhat limited; a mixing factor (m) is generally employed to modify the equations for a well-mixed model to account for the nonuniform distribution of concentration. It is usually preferable for these types of problems to employ CFD techniques and numerical models for dispersive transport.

5.1 Analytical Tools

Assume an enclosed space exists in which the concentration is considered to be spatially uniform. The mass concentration at $t = 0$ is c_0 . A source begins to generate contaminants at a constant rate (S). Outside air with contaminant c_a is

added to the enclosure at a constant volumetric flow rate Q – contaminated air is removed from the space at the same rate. Applying the equation for conservation of mass, the governing equations for the contaminant concentration entering and leaving the enclosure can be written as

$$V \frac{dc}{dt} = Qc_a - Qc + S \quad (46)$$

where V is the volume of the enclosure. Since the flow of air into and out of the enclosure is balanced, one only needs the expression for c . Integrating over time,

$$\int_{c_0}^{c(t)} \frac{dc}{[(Qc_a + S) - Qc]} = \frac{1}{V} \int_0^t dt \quad (47)$$

Solution of Equation (46) is

$$\frac{(c_{ss} - c(t))}{(c_{ss} - c_0)} = \exp\left(-\frac{Qt}{V}\right) \quad (48)$$

where c_{ss} is the steady state concentration (where $c_{ss} = c_a + S/Q$) obtained by setting the LHS of Equation (46) equal to zero. Assuming both initial and ambient concentrations are zero, one obtains the reduced form of Equation (48)

$$\frac{c(t)}{c_{ss}} = 1 - \exp(-Nt) \quad (49)$$

where $N = Q/V$ and is known as the number of room air changes per minute. To illustrate, if the ventilation rate is 10 room changes per hour, Equation (49) predicts that the concentration will be 64% of its steady state value in 6 minutes.

For a time-varying source or ventilation flow rate, Equation (46) can be rewritten as

$$\frac{dc}{dt} = -\frac{Qc}{V} + \frac{(S + Qc_a)}{V} \quad (50)$$

Equation (50) must be solved iteratively. Using a simple Runge-Kutta method, Equation (50) can be solved using the expression

$$c^{n+1} = \frac{\left(1 + \frac{A\Delta t}{2}\right)c^n + B\Delta t}{1 - \frac{A\Delta t}{2}} \quad (51)$$

where i is the iteration, $A = -Q/V$, $B = (S + Qc_a)/V$, and Δt is the time step. The solution begins with $t = 0$ and $i = 0$ where c_o is the initial concentration.

To account for wall losses (i.e., removal of contaminant by solid surfaces), Equation (46) can be modified to include the adsorption rate (k_{ad}) of contaminant on walls

$$V \frac{dc}{dt} = Qc_a + S - c(Q + A_s k_{ad}) \quad (52)$$

Equation (52) can be integrated to give

$$\frac{(c_{ss} - c(t))}{(c_{ss} - c_o)} = \exp\left(-\frac{(Q + A_s k_{ad})t}{V}\right) \quad (53)$$

assuming constant values for Q , S , and k_{ad} . For the case when $Q = S = 0$ (starting with a room contaminated), Equation (53) can be modified to

$$\frac{c(t)}{c_{max}} = \exp\left(-\frac{A t k_{ad}}{V}\right) \quad (54)$$

where c_{max} represents the maximum concentration at the beginning of the integration. Figure 3 shows the importance of adsorption of tobacco smoke (see Repace and Lowery, 1980; Heinsohn, 1991) and the effects of mixing in a room. In this instance, a single cigarette was burned and then extinguished in a 22 m³ room and the total mass of suspended particle matter measured during the entire period. Well-mixed conditions were produced by fans; the natural mixing occurred as a result of natural air currents. Notice that the concentration in the well-mixed experiment fell rapidly, as expected. The slope of the curve allows one to estimate the removal of contaminants by adsorption on solid surfaces. The rate of adsorption was found to be equivalent to an exhaust ventilation rate of 1.4 m³/min (50 CFM). It should also be pointed out that contaminants can also *desorb* from surfaces. In this case, desorption acts as a source term in Equation (48).

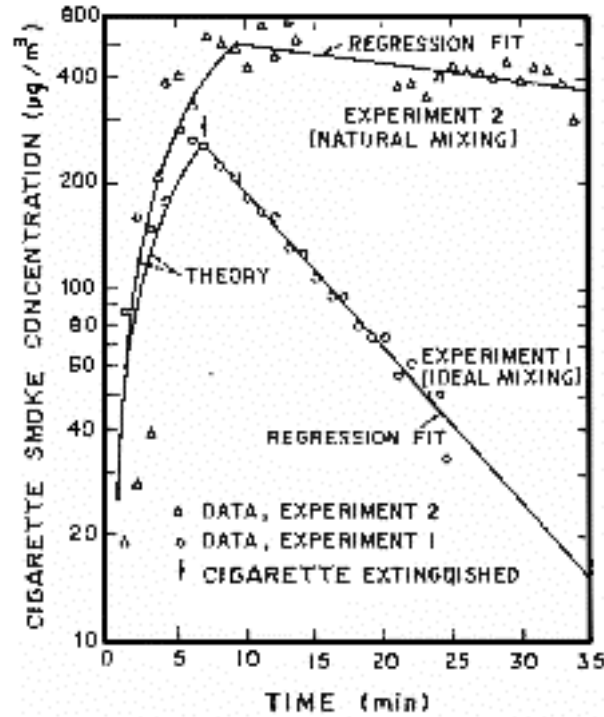


Figure 3. Smoke concentration within a room with and without internal mixing (from *Industrial Ventilation*, R. J. Heinsohn, J. Wiley & Sons, New York, 1991, pg. 245).

If only a fraction (f) of the return flow into an enclosed space is fresh air, Equation (46) can be modified to the following form

$$V \frac{dc}{dt} = -cQ[1 - (1-f)(1-\eta)] + S + Qfc_a(1-\eta) \quad (55)$$

where f is the makeup air fraction (makeup of fresh air/input air) and η is the efficiency of the air cleaning device. Integrating Equation (55),

$$\frac{(c_{ss} - c(t))}{(c_{ss} - c_o)} = \exp \left[- \left(\frac{Qt}{V} \right) \{1 - (1-\eta)(1-f)\} \right] \quad (56)$$

For variable source or volumetric flow rates, Equation (55) must be solved numerically.

For partially mixed conditions, the concentration varies both spatially and temporally. This condition is normally found in most industrial applications. The technique employed here is to introduce a mixing factor (m) to account for the spatial variations in concentration. Equation (46) now becomes

$$V \frac{dc}{dt} = S + (mQc_a) - (mQc) - (mc\eta Q_r) \quad (57)$$

where Q_r is the volumetric flow rate of recirculated air. Integration of Equation (57) gives

$$\frac{(c_{ss} - c(t))}{(c_{ss} - c_o)} = \exp\left[-\frac{mt(Q + Q_r\eta)}{V}\right] \quad (58)$$

For this particular type of situation, setting $m = 1$ indicates a well-mixed model while $m < 1$ implies nonuniform mixing and spatial variations in concentration (i.e., $m = 0.5$ is used for a perforated ceiling, $m = 0.166$ is for natural draft and ceiling exhaust fans, $m = 0.10$ is used for infiltration and natural drafts).

The source emission rate, or source strength (S), is usually not known and must be determined from experiment. A source can be released in a clean room and measurements made of the rise in concentration. The governing equation is

$$V \frac{dc}{dt} = S - c(Q_s + A_s k_{ad}) \quad (59)$$

where Q_s represents the volumetric flow rate through the sampling device. Immediately after the source is activated and while the concentration is small, Equation (59) reduces to the simple form

$$V \frac{dc}{dt} = S \quad (60)$$

and the source strength can be found from the slope of concentration versus time. A more accurate means of determining S is to measure two concentrations, c_1 and c_2 at two times t_1 and t_2 , and obtain S from the integration of Equation (59), i.e.,

$$S = -(A_s k_{ad} + Q_s) \left[c_1 \exp\left(\frac{-(A_s k_{ad} + Q_s)(t_2 - t_1)}{V}\right) - c_2 \right] / G \quad (61)$$

$$G = 1 - \exp\left[\frac{-(A_s k_{ad} + Q_s)(t_2 - t_1)}{V}\right]$$

Example:

An exhaust hood is installed within a few feet of a makeup air inlet in a room. Ethyl alcohol is evaporated in the hood. What is the steady state concentration of ethyl alcohol in the room and the amount of time before one begins to smell alcohol? Assume the threshold odor limit for ethyl alcohol is 40 mg/m^3 and the following criteria apply:

- V = volume of operating room (50 m^3)
 A_s = total area of adsorbing surfaces in operating room (85 m^2)
 k_{ad} = adsorption rate constant (0.001 m/s)
 S = rate at which ethyl alcohol is vaporized inside operating room
 (1 g/min)
 c_o = initial alcohol concentration inside operating room (10 mg/m^3)
 c_a = concentration of ethyl alcohol entering the makeup air duct
 (100 mg/m^3)
 Q_e, Q_r, Q_a, Q_s = volumetric flow rate of exhausted air, recirculated air,
 makeup air, and supply air ($Q_s = 20 \text{ m}^3/\text{min}$)
 $f = Q_a/Q_s$ = make up air fraction (0.9)
 η_1, η_2 = efficiencies of activated charcoal filter (0.5)

The governing equation to be solved is of the form

$$V \frac{dc}{dt} = S + Q_s c_s - c Q_e - c A_s k_{ad} \quad (62)$$

A mass balance for the air results in the expression

$$\begin{aligned} Q_s &= Q_a + Q_r \\ Q_e &= Q_s \end{aligned} \quad (63)$$

At the fan inlet, the mass balance for alcohol is

$$c_a Q_a (1 - \eta_2) + c Q_r (1 - \eta_1) = c_s Q_s \quad (64)$$

Using the definition of f ,

$$c_s = c_a f (1 - \eta_2) + c_r (1 - \eta_1) (1 - f) \quad (65)$$

The differential equation to be solved is of the form

$$\frac{dc}{dt} = Ac + B \quad (66)$$

where A and B are evaluated as

$$\begin{aligned} A &= \frac{\{-Q_s - A_s k_{ad} + Q_s (1 - f) (1 - \eta_1)\}}{V} = -\frac{25 \text{ m}^3 / \text{min}}{50 \text{ m}^3} = -0.5 \text{ min}^{-1} \\ B &= \frac{[S + f Q_s c_a (1 - \eta_2)]}{V} = 0.0218 \text{ g} / \text{m}^3 \text{ min} \end{aligned} \quad (67)$$

Setting $dc/dt = 0$ gives the steady state concentration,

$$c_{ss} = -\frac{B}{A} = 45.6 \text{ mg/m}^3 \quad (68)$$

Since A and B are known constants, the time can be calculated from the integral expression

$$\int_{10}^{40} \frac{dc}{[Ac + B]} = \int_0^t dt \quad (69)$$

$$t = 4.47 \text{ min}$$

5.2 Advection Model

Often, a source exists that is moving within a confined space. Examples of such situations are automobiles that are traveling through tunnels or a smoker walking from one room to another. In this instance, a simple control volume approach can be used to establish the governing equation for concentration. In many instances, make-up air consisting of fresh air is used to provide local ventilation, e.g., for tunnels less than 600 m in length.

A schematic of air and contaminant transport within a tunnel is shown in Figure 4. An elemental volume denoted by $A dx$ exists within a tunnel with uniform make-up air and exhausts. The conservation of mass for air within the volume gives the following expression

$$\frac{dU}{dx} = q_m - q_e \quad (70)$$

where $q_m = Q_m/LA$ and $q_e = Q_e/LA$. If q_m and q_e are constant, the air velocity in the tunnel at any location x is

$$\frac{U(x)}{U_o} = 1 + \frac{x(q_m - q_e)}{U_o} \quad (71)$$

where U_o denotes air entering the tunnel. If $q_m > q_e$, then $U(x)$ increases linearly with x ; if $q_e > q_m$, $U(x)$ decreases. The conservation of mass for contaminants can be written as

$$c \frac{dU}{dx} + U \frac{dc}{dx} = s + q_m c_m - c q_e - kc \quad (72)$$

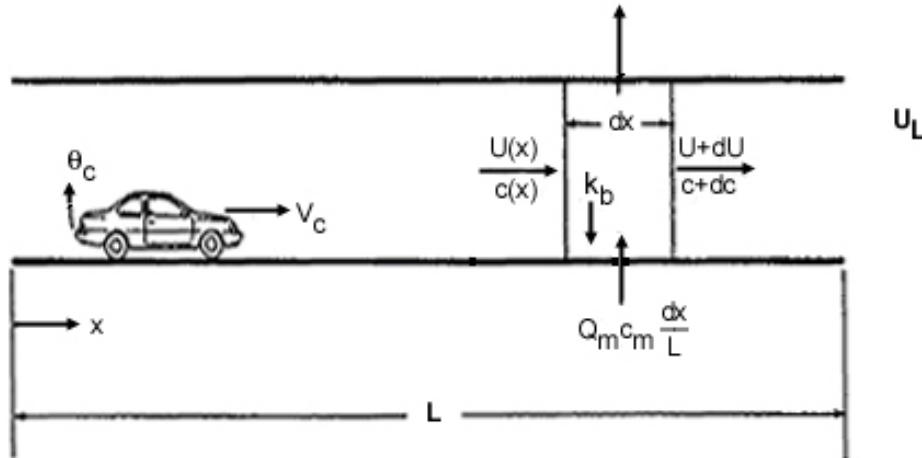


Figure 4. Air and concentration within a tunnel (from *Industrial Ventilation*, R. J. Heinsohn, J. Wiley & Sons, New York, 1991, pg. 567).

where $s = S/LA$ ($\mu\text{g}/\text{m}^3\text{-min}$) and $k = 4k_d/D$ (min^{-1}). D is the tunnel diameter, c_m is the contaminant, S is the source (mg/hr), and k_d (m/s) is the rate at which contaminant is deposited on the tunnel walls. Combining Equations (71)-(72), the equation for contaminant within the tunnel is

$$U \frac{dc}{dx} = s + q_m c_m - c(k + q_m) \quad (73)$$

which can be rewritten using Equation (71) as

$$\frac{dc}{(q_m c_m + s) - (k + q_m)c} = \frac{dx}{U_o + (q_m - q_e)x} \quad (74)$$

If q_m and q_e are constant (unequal and nonzero), Equation (74) can be integrated to

$$c(x) = \frac{s + q_m c_m}{k + q_m} + \left[c_o - \left(\frac{s + q_m c_m}{k + q_m} \right) \right] \left[\frac{U(x)}{U_o} \right]^{-b} \quad (75)$$

where $b = (k + q_m)/(q_m - q_e)$ and $U(x)/U_o$ can be replaced using Equation (71). If q_e and q_m vary with x , Equation (74) must be solved using a numerical approach, e.g., Runge-Kutta. If q_e and q_m are zero, Equation (74) cannot be used and Equation (73) must be integrated directly. When q_e and q_m are equal, the system is balanced. The usual case is for $q_m > q_e$.

5.3 Box Model

When the concentration within an enclosure is nonuniformly distributed, it is inaccurate to assume the enclosure can be treated as a well-mixed region. Although one could utilize partially mixed conditions and use mixing factors, the uncertainty in selecting values for m and the tendency of the partially mixed model to still predict spatially uniform concentrations would likely result in large inaccuracies. An alternative approach to the analytical tools utilized in the previous section is the *box model*, also sometimes referred to as the multi-cell well-mixed model (Heinsohn, 1991). Figure 5 shows a schematic of a partially mixed enclosure with two sources, two makeup air vents and two exhaust vents.

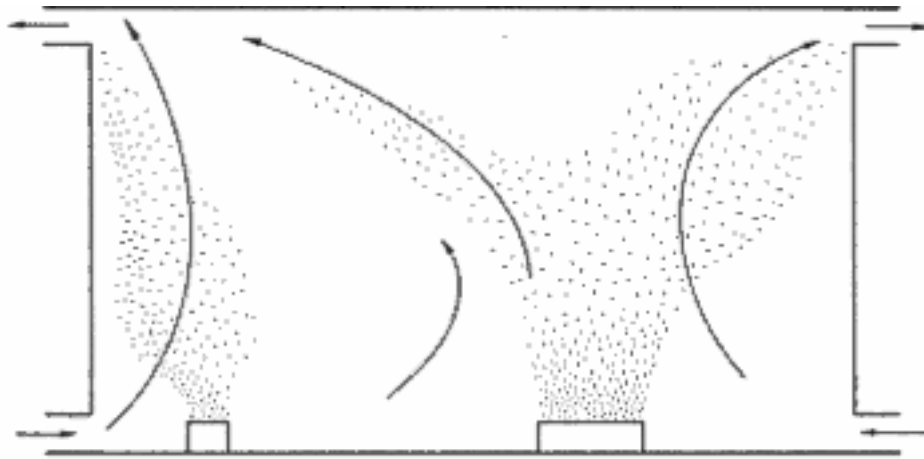


Figure 5. Partially mixed enclosure with two sources, two makeup air vents, and two exhaust vents (from *Industrial Ventilation*, R. J. Heinsohn, J. Wiley & Sons, New York, 1991, pg. 265).

Utilizing a box model approach, the domain is divided into two cells with contaminant that transfers between each cell. This is shown in Figure 6 for the two-cell model; the user can implement as many cells as desired – in this case, the problem domain is ideal for establishing a two-cell approach.

We begin by introducing the volumetric flow rates (Q) and fractions of those rates entering (x) and leaving (y) the cell boundaries.

Entering the enclosure:

$$\begin{aligned}
 Q_{1,i} &= x_1 Q \\
 Q_{2,i} &= x_2 Q \\
 Q &= Q_{1,i} + Q_{2,i} = Q(x_1 + x_2) \\
 x_1 + x_2 &= 1
 \end{aligned}
 \tag{76}$$

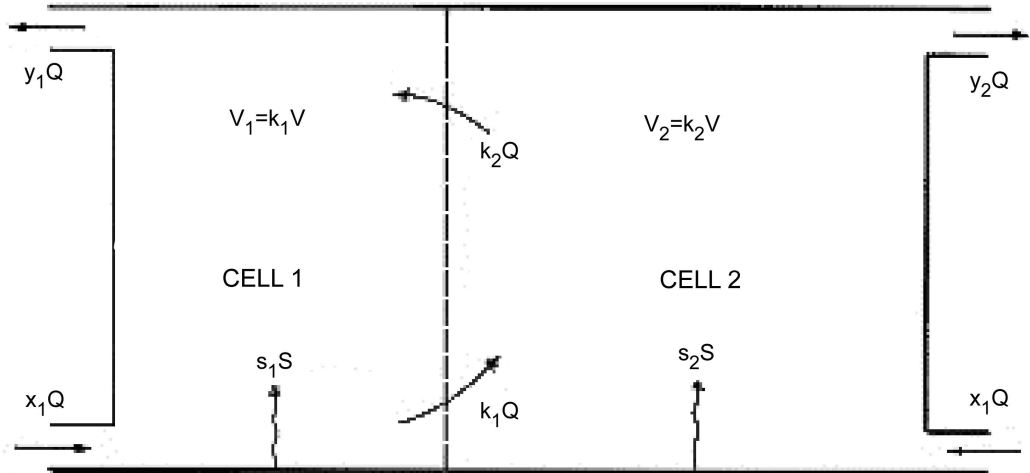


Figure 6. Two-cell box model (adapted from *Industrial Ventilation*, R. J. Heinsohn, J. Wiley & Sons, New York, 1991, pg. 266).

Leaving the enclosure:

$$\begin{aligned} Q_{1,o} &= y_1 Q \\ Q_{2,o} &= y_2 Q \\ y_1 + y_2 &= 1 \end{aligned} \quad (77)$$

The fractions are obtained from knowing the amounts of make-up air, recirculation, exhaust, and infiltration. The fraction of contaminant in each cell is designated as s_1 and s_2 , i.e.,

$$\begin{aligned} S &= S(s_1 + s_2) \\ s_1 + s_2 &= 1 \end{aligned} \quad (78)$$

and the volume of cells 1 and 2 expressed as fractions, v_1 and v_2 , of the total volume, V , as

$$\begin{aligned} V &= V(v_1 + v_2) \\ v_1 + v_2 &= 1 \end{aligned} \quad (79)$$

Fractional values for x , y , s , and v are input by the user.

The amount of volumetric flow rate transferred across the internal boundary between cells 1 and 2 is denoted through the use of exchange coefficients, k_1 and k_2 , which can vary from less than to greater than 1. Performing a conservation of mass balance yields the following expressions for cell 1 and 2,

$$\begin{aligned}
\text{Cell 1: } x_1Q + k_2Q - y_1Q - k_1Q &= 0 \\
x_1 - y_1 + k_2 - k_1 &= 0 \\
\text{Cell 2: } x_2Q + k_1Q - y_2Q - k_2Q &= 0 \\
x_2 - y_2 + k_1 - k_2 &= 0
\end{aligned} \tag{80}$$

The governing equations for the conservation of mass become

$$\begin{aligned}
v_1V \frac{dc_1}{dt} &= s_1S + x_1Qc_a + k_2Qc_2 - k_1Qc_1 - y_1Qc_1 \\
v_2V \frac{dc_2}{dt} &= s_2S + x_2Qc_a + k_1Qc_1 - k_2Qc_2 - y_2Qc_2
\end{aligned} \tag{81}$$

where c_a is the concentration in the air entering cells 1 and 2. The two sets of relations described by Equation (81) can be rewritten to the simpler pair of simultaneous, first-order differential equations by assuming $v = v_l$, $s = s_l$, and $k = k_l$ (and thus $k_2 = k + y - x$)

$$\begin{aligned}
\frac{dc_1}{dt} &= A + Bc_1 + Dc_2 \\
\frac{dc_2}{dt} &= E + Fc_2 + Gc_1
\end{aligned} \tag{82}$$

where the coefficients are defined as

$$\begin{aligned}
A &= \left(\frac{N}{v}\right) \left[x_1c_a + \left(\frac{sS}{Q}\right) \right]; \quad B = -\left(\frac{N}{v}\right) [k + y_1] \\
D &= \left(\frac{N}{v}\right) [x_2 - y_2 + k]; \quad E = \left(\frac{N}{(1-v)}\right) \left[x_2c_a + \left\{ (1-s) \frac{S}{Q} \right\} \right] \\
F &= -\left(\frac{N}{(1-v)}\right) [x_2 + k]; \quad G = \frac{Nk}{(1-v)}; \quad N = \frac{Q}{V}
\end{aligned} \tag{83}$$

The general solution to the pair of relations defined by Equations (82)-(83) is

$$\begin{aligned}
c_1(t) &= K_1 \exp(Ntw_1) + K_2 \exp(NTw_2) + c_{1,ss} \\
c_2(t) &= MK_1 \exp(Ntw_1) + LK_2 \exp(NTw_2) + c_{2,ss}
\end{aligned} \tag{84}$$

where $c_{1,ss}$ and $c_{2,ss}$ are the final (steady state) cell concentrations given as

$$c_{1,ss} = \frac{AF - ED}{DG - BF}; \quad c_{2,ss} = \frac{EB - AG}{DG - BF} \tag{85}$$

where

$$\begin{aligned}
 w_1 &= \left(\frac{1}{2N} \right) \left[(B+F) + \sqrt{(B-F)^2 + 4DG} \right] \\
 w_2 &= \left(\frac{1}{2N} \right) \left[(B+F) - \sqrt{(B-F)^2 + 4DG} \right] \\
 M &= \frac{Nw_1 - B}{D}; \quad L = \frac{Nw_2 - B}{D} \\
 I_1 &= c_1(0) - c_{1,ss}; \quad I_2 = c_2(0) - c_{2,ss} \\
 K_1 &= \left[L - \left(\frac{I_2}{I_1} \right) \right] \left[\frac{I_1}{(L-M)} \right]; \quad K_2 = \left[\left(\frac{I_2}{I_1} \right) - M \right] \left[\frac{I_1}{(L-M)} \right]
 \end{aligned} \tag{86}$$

where $c_1(0)$ and $c_2(0)$ are the initial cell concentrations. It is a simple matter to solve for the equation pair established by Equation (82). The only difficulty is in selecting an appropriate value for the exchange coefficient, k , which is difficult to establish. The best way is to use trial and error or some empirical judgment to determine a range of values for k . Note that as the value of k increases, the exchange between cells increases. When k reaches a value of around 15, the concentration in both cells approaches the equivalent of a single well-mixed cell, i.e., well-mixed conditions can be assumed throughout the entire enclosure. Although using two cells is crude, it is much better than assuming well-mixed conditions for the problem domain. Of course, one can always add more cells in an effort to refine the problem details and obtain a more accurate solution; however, the complexity of analyzing multiple cells increases proportionally to the square of the number of cells. If one winds up using many cells, it may be best to ultimately go to the use of numerical methods, i.e., CFD. The accuracy of the box model is limited by the inability to establish enough detail to describe the exchange of air among cells, especially if transient solutions are sought.

Box Model Example

Objects are to be cleaned in HCl solutions in one room before final assembly in an adjacent room. The liquid surface area is 75 ft² and HCl vapor is emitted at a rate of 0.02 gm/s-m². The room with HCl is 30 ft x 30 ft x 15 ft and has a doorway 10 ft x 15 ft into the adjacent room that is 50 ft x 30 ft x 15 ft. No HCl is generated in the adjacent room. The plant manager has reservations that placing an air curtain in the doorway will prevent HCl vapor from entering the adjacent room. Each room has its own HVAC system. Each room is well mixed and infiltration and exfiltration are equal to one change per hour. The ventilation system delivers 600 CFD of outside air to the adjacent room and 600 CFD of contaminated air is removed from the room containing HCl. What are the steady state concentrations in each room, how fast do the concentrations increase in time, and is the PEL (5 ppm ~ 7 mg/m³) exceeded in each room? Assume that no adsorption occurs and that HCl is initially zero.

Utilizing Equations (81)-(86), the following values for the various constants, assuming a two cell model, are calculated as shown in Table 11.

Table 11. Values for various parameters used in box model example.

Parameter	Value
x_1	0.1875
x_2	0.8125
y_1	0.6875
y_2	0.3125
S	1.0
V	0.375
Q	72,000 CFM
S	502 gm/hr
N	2 hr^{-1}
A	0.0372 gm/hr-m^3
B	$-5.33 (k+0.6875) \text{ hr}^{-1}$
D	$5.33 (k+0.5) \text{ hr}^{-1}$
E	0
F	$-3.2 (k+0.8125) \text{ hr}^{-1}$
G	$3.2 (k) \text{ hr}^{-1}$

Using Equation (71), a steady state concentration value of 175 ppm is obtained with a time constant of 0.5 hr, using a value of $k = 15$ (which is very conservative but allows one to place an upper bound on the exchange). Using this upper limit, the PEL would be exceeded during the working day. Figure 7 shows concentration values versus time within the two cells using $k = 0.2$ and $k = 1.8$. If $k = 0$, cell 1 is well mixed and cell 2 receives no HCl; as k increases, mixing increases. Steady state concentrations in both rooms approach values that would be predicted assuming well-mixed conditions throughout the rooms.

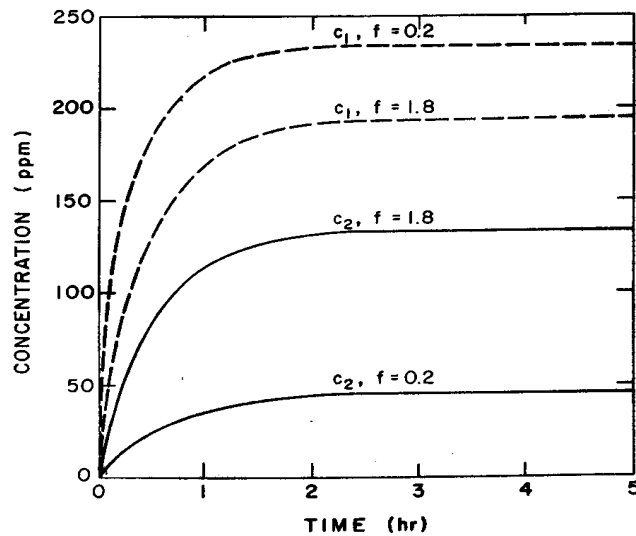


Figure 7. Box model example for mixing of HCL between two rooms (from *Industrial Ventilation*, R. J. Heinsohn, J. Wiley & Sons, New York, 1991, pg. 270).

6 Dynamics of Particles and Gases/Vapors

6.1 Drag, Shape, and Size of Particles

Analyzing the force on a particle in a flow field reveals the fluid to be exerting a force proportional to the particle's projected area, the square of the relative velocity of the particle to the fluid. This proportionality is known as Newton's resistance equation. In general form, Newton's resistance equation is

$$F_d = C_d \frac{\pi}{8} \rho_f d_p V^2 \quad (87)$$

where V is the relative velocity of the particle with diameter d_p having a drag coefficient C_d in a fluid with density ρ_f . This equation is valid for particle motion at subsonic speeds. Particles having Reynolds number (Re) less than one, $Re = d_p V \rho_f / \mu \ll 1$, the Stokes regime, the drag force is

$$F_d = 3\pi\mu d_p V \quad (88)$$

When substituted into Equation (87), the coefficient of drag is $C_d = 24 / Re$.

If particle size is of the order of the molecular mean free path, the particle no longer experiences the fluid as a continuum, but as individual molecules. Particles of this size invalidate the assumption of a no-slip boundary condition for the fluid on the particle's surface used in the Stokes flow analysis. The particle is able to slip through the fluid, reducing the drag experienced by the particle as predicted from a continuum analysis in Stokes' flow regimes. A slip factor (Cunningham slip correction factor) for particle drag factor corrects the Stokes drag coefficient

$$C_c = 1 + (2\lambda / d_p)(A_1 + A_2 e^{-A_3 d_p / \lambda}) \quad (89)$$

The variable λ is the molecular mean free path and is given by (Cooper and Alley, 1994)

$$\lambda = \frac{\mu}{0.499P \sqrt{8MW_f / \pi R T}} \quad (90)$$

where μ is the absolute viscosity of the fluid, MW_f is the molecular weight of the fluid, R is the universal gas constant, P is the pressure, and T is the absolute temperature. Any consistent set units will provide the length of the mean free path. The factors A_1, A_2, A_3 are dimensionless empirical constants for small particle drag (Martin et al., 1983).

The slip factor is used to augment the coefficient of drag in the force equation. The force of drag becomes

$$F_d = \frac{3\pi\mu V d_p}{C_c} \quad (91)$$

Particles of various shape and size are found in the indoor environment. Depending the molecular structure of the mineral or molecules forming the particle, it is possible to predetermine the shapes expected from some compounds (e.g., salt has a cubical shape and fibers are cylindrical in shape).

The Newton's resistance equation and Stokes flow analysis can be adjusted to account for non-spherical particles. By using an equivalent volume for the particle, that is, creating a sphere of equivalent volume that an irregular shaped particle would have if it were spherical, Stokes law becomes

$$F_d = 3\pi\mu V d_{pe} \quad (92)$$

where d_{pe} is the equivalent diameter of the particle.

An aerodynamic diameter is an equivalent diameter that is defined as the diameter of a spherical water droplet (a spherical particle with unit density) which has the same settling velocity v_s as the particle. The mathematical relation for aerodynamic diameter is

$$d_a = \sqrt{\frac{18\mu v_s}{C_c \rho_{\text{water}} g}} \quad (93)$$

Any equivalent set of units can be used to determine the aerodynamic diameter. The settling velocity, a terminal velocity of a particle in calm air, is determined by solving a particle's steady state rectilinear motion in a gravitational field, that is, by solving

$$F_g - F_d = m_p \frac{dv_p}{dt} \quad (94)$$

where F_g is the gravitational force exerted on the particle having mass m_p . Then solving this differential equation for the particles velocity, v_p , at steady state yields a terminal settling velocity

$$v_s = \frac{\rho_p d_p^2 C_c}{18\mu} g \quad (95)$$

6.2 Particle Motion

When the number of particles in the air is low, it is fair to assume that the particles do not influence the velocity field of the air. In other words, the average distance between any two particles is at least 10X the particle diameter. For water droplets, this would correspond to less than 4.2 kg/m³ in air. Table 12 shows upper limits for particle concentration influence on the flow field based on particle diameter and number density.

Table 12. Particle diameter versus density for influencing flow field.

Diameter (μm)	particles/m ³
1.0	8 x 10 ¹⁵
10.0	8 x 10 ¹²
100.0	8 x 10 ⁹

If knowledge of the velocity field of the air (or carrier gas) is known, then particle trajectories can be calculated. For situations when the density of a particle is 1000X greater than the density of air, buoyancy on a particle can be neglected. The motion of a single spherical particle can be expressed using the relation

$$\left(\frac{\pi D_p^3}{6}\right)\rho_p \frac{d\mathbf{v}}{dt} = -\left(\frac{C_D \rho}{2C}\right)\left(\frac{\pi D_p^2}{4}\right)(\mathbf{v} - \mathbf{U})|\mathbf{v} - \mathbf{U}| - \left(\frac{\pi D_p^3}{6}\right)\rho_p \mathbf{g} \quad (96)$$

where \mathbf{v} is the velocity of the particle, \mathbf{U} is the air velocity, C is a slip factor (~ 1 for $D_p \geq 10\mu\text{m}$), and \mathbf{g} is acceleration of gravity. Equation (96) is useful when calculating freely falling particles due to gravimetric settling, horizontal motion in quiescent air, and particles traveling through a moving stream.

For a particle settling in quiescent air ($\mathbf{U} = 0$) due to gravitation, motion is only downward. Hence, the vector velocity becomes $\mathbf{v} \equiv -v$ (where v denotes vertical motion). Likewise, the drag coefficient becomes $C_D = 24\mu/\rho D_p v$. Equation (96) can be simplified to the following form,

$$\frac{dv}{dt} = g - \frac{v}{\tau C} \quad (97)$$

where $\tau = \rho_p D_p^2 / 18\mu$, which is known as the relaxation time. If the particle starts from rest, the downward velocity is

$$v(t) = Cg\tau \left[1 - \exp\left(-\frac{t}{\tau C}\right) \right] \quad (98)$$

If $t \gg \tau$, then the settling, or terminal velocity (v_t), of the particle can be calculated using the simple relation

$$v_t = \tau g C \quad (99)$$

assuming that the Reynolds number ($Re = \rho U D_p / \mu$) is low. Figure 8 shows particle diameter versus settling velocity for three specific gravities (SG). Note that the settling velocity varies as the square of the particle diameter when $Re \leq 1$.

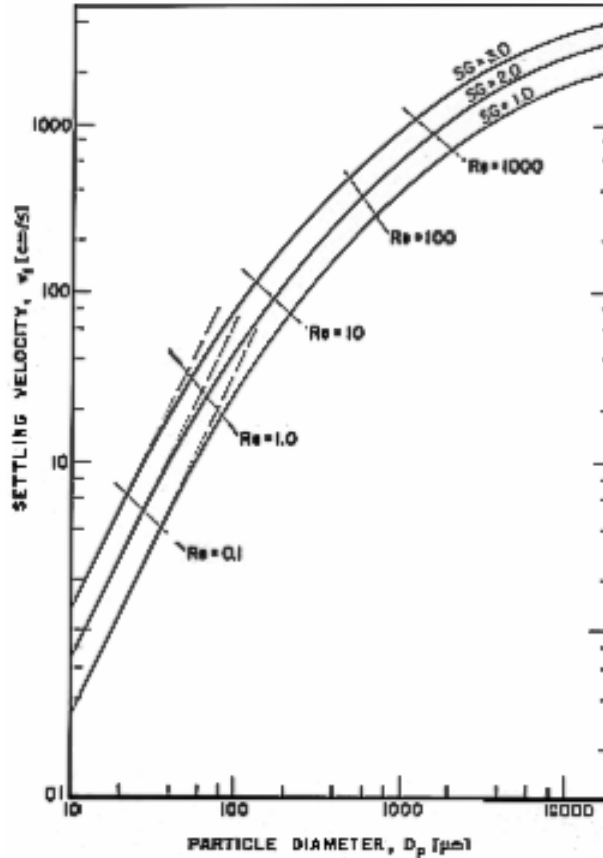


Figure 8. Settling velocity of spherical particles for three specific gravities (from *Industrial Ventilation*, R. J. Heinsohn, J. Wiley & Sons, New York, 1991, pg. 450).

When the particle is very large and $Re > 1000$, $C_D \sim 0.4$ and the settling velocity can be found from the relation

$$v_t = \sqrt{\left(\frac{4}{3}\right) \left(\frac{\rho_p D_p g}{0.4 \rho}\right)} \quad (100)$$

For a particle moving horizontally in quiescent air, we will assume that the horizontal velocity (u) of a sphere occurs when $Re \leq 1.0$. The differential equation for the horizontal motion is

$$\frac{du}{dt} = -\frac{u}{\tau C} \quad (101)$$

which can be integrated to yield

$$u(t) = u(0) \exp\left[-\frac{t}{\tau C}\right] \quad (102)$$

and the horizontal displacement (also known as stopping or penetration distance) calculated as

$$\int_0^{x(t)} dx = \int_0^t u dt = \tau C u(0) \left[1 - \exp\left(-\frac{t}{\tau C}\right)\right] \quad (103)$$

The maximum stopping distance is easily found by allowing $\tau \gg t$.

For particles traveling in a 2-D moving air stream, Equation (96) must be modified to the form

$$\frac{d\mathbf{v}}{dt} = -\left(\frac{3C_D}{4C}\right) \left(\frac{\rho}{\rho_p D_p}\right) (\mathbf{v} - \mathbf{U}) |\mathbf{v} - \mathbf{U}| - \mathbf{g} \quad (104)$$

which can be reduced to the following pair of coupled differential equations,

$$\begin{aligned} \frac{du}{dt} &= -\left(\frac{3C_D}{4C}\right) \left(\frac{\rho}{\rho_p D_p}\right) u_r (u_r^2 + v_r^2)^{1/2} \\ \frac{dv}{dt} &= -\left(\frac{3C_D}{4C}\right) \left(\frac{\rho}{\rho_p D_p}\right) v_r (u_r^2 + v_r^2)^{1/2} - g \end{aligned} \quad (105)$$

where u_r and v_r are relative velocities ($u-U$; $v-U$) and

$$C_D = 0.4 + \frac{24}{Re} + \frac{6}{(1 + Re^{1/2})}$$

$$Re = \rho D_p \frac{[u_r^2 + v_r^2]^{1/2}}{\mu}$$
(106)

For the case when the particle's motion is in a flow regime where $Re \leq 1.0$, the pair of equations reduce to the much simpler form

$$\frac{du}{dt} = -\left(\frac{u - U_x}{\tau C}\right)$$

$$\frac{dv}{dt} = -\left(\frac{v - U_y}{\tau C}\right) - g$$
(107)

which can be integrated, assuming $u(0) = v(0) = 0$, to

$$u(t) = u(0) \exp\left[-\frac{t}{\tau C}\right] + U_x(0) \left[1 - \exp\left(-\frac{t}{\tau C}\right)\right]$$

$$v(t) = v(0) \exp\left[-\frac{t}{\tau C}\right] - (g\tau C) \left[1 - \exp\left(-\frac{t}{\tau C}\right)\right]$$
(108)

where U_x and U_y denote components of the air velocity in the horizontal and vertical directions, respectively. If Re values are unknown and the flow regime is well beyond low flow levels, numerical methods (CFD) are required to compute the particle velocities and trajectories.

Particle motion is described by the time dependent convection-diffusion equation. For inviscid analysis or in laminar flow the transport equation can be easily adjusted to account for settling by incorporating a settling velocity into the advection-diffusion equation.

6.2.1 Deposition of Particulate with Aerodynamic Diameters $> 1\mu$ by Settling

The deposition of large particles by diffusion is extremely small as is evident by examining the equation for the velocity of deposition through a boundary layer of thickness δ_{part} , from diffusion alone. In the absence of thermophoretic velocities and turbulent dispersion, deposition velocity is a function of gravitational settling. The equation for species transport with settling becomes

$$\frac{\partial C_j}{\partial t} + u \frac{\partial C_j}{\partial x} + (v - v_{s_j}) \frac{\partial C_j}{\partial y} + w \frac{\partial C_j}{\partial z} = \frac{D_j}{\rho} \left[\frac{\partial^2 C_j}{\partial x^2} + \frac{\partial^2 C_j}{\partial y^2} + \frac{\partial^2 C_j}{\partial z^2} \right] + Q_c \quad (109)$$

This equation has a different advective velocity term in the y coordinate or direction of gravitational influence from Equation 1. The advective term $v - v_s$ in Equation (109) represents some relaxation of the particulate velocity versus the free stream velocity.

The deposition rate is given by

$$J = v_s \rho_p \quad (110)$$

For particles larger than $10 \mu\text{m}$ and Reynolds number between 2 and 500, the settling velocity is defined as (Cooper and Alley, 1994)

$$v_s = \frac{0.153 d_p^{1.14} \rho_p^{0.71} g^{0.71}}{\mu \rho^{0.29}} \quad (111)$$

Inertial deposition from laminar flow occurs for larger particles, which may be carried from the streamline flow onto an obstruction. The distance the particle would be carried from the streamline is dependent on the particle's momentum and size. The trajectory of the particle is initially a function of the fluid's trajectory.

Consider a distance a particle will travel from its inertia. Let that distance be just to a surface, a stopping distance of d_s . The velocity v_s of the particle normal to the surface multiplied by the time t , the relaxation time, is the stopping distance $d_s = v_s t$.

The rate of deposition from this stopping distance is determined by the concentration of particles with this relaxation time. As the particle size decreases, the distance traveled from inertia decreases, that is, the relaxation time is decreased. Relaxation time is defined as

$$t = \frac{C_c \rho_p d_p^2}{18\mu} \quad (112)$$

The particulate flux from the stopping distance d_s is

$$J_s = v_s C_j |_{d_s} \quad (113)$$

The value of C_j , is the value of the concentration at the stopping distance for that particular particulate density and size.

Inertial forces on large particles in turbulent flow are important mechanisms for deposition by impingement. Larger particles are carried into the boundary layer by inertia. The distance particles are carried into the transitional and laminar sublayers depends on the stopping distance which is dependent on the following factors: 1) particle size, 2) particle mass, and 3) degree of turbulence or energy of the flow.

If molecular diffusion is neglected, the velocity of deposition for particles is given by

$$V_{d+} = \frac{\mu_{\text{turb}}}{v_{\text{fluid}}} \frac{dc_+}{dy_+} = \frac{V_d}{u_*} \quad (114)$$

This equation is true for one-dimensional flow towards a flat plate. This equation provides a good approximation to flow within a cylinder where the radius of a surface is large compared to the scale of the turbulent boundary layer (Davies, 1966).

Consider, a particle travel distance just to a surface as the stopping distance of d_{s+} with a turbulent velocity v_{s+} normal to the surface, then

$$d_{s+} = v_{s+} t_+ \quad (115)$$

where $t_+ = t u_*^2 / \nu$ is the nondimensional relaxation time. The rate of deposition from this distance is determined by the concentration of particles with this relaxation time. As the particle size decreases, the distance traveled from inertial forces decreases, that is, the relaxation time is decreased. Relaxation time is defined as

$$t = \frac{C_c \rho_p d_p^2}{18\mu} \quad (116)$$

The non-dimensional particulate flux from the stopping distance d_{s+} is $J_{s+} = v_{s+} c_+|_{d_{s+}}$. The value of c_+ is the value of the concentration at the stopping distance for that particular particulate density and size.

6.2.2 Particle Motion in Electrostatic Field

Electrostatic forces can have very significant influence on the motion of aerosols. Most airborne particles are electrically charged, and when in the presence of electric potential, the resulting forces on the particles cause significant motion. So much so that this force is utilized by electrostatic precipitators for air cleaning and by aerosol measurement instruments.

Coulomb's law describes the electrostatic force as

$$F_e = \frac{1}{4\pi\epsilon_0} \frac{q_1 q_2}{r_{12}^2} \quad (117)$$

where q_1 is the particle's charge, q_2 is the surface's charge (or other point source), ϵ_0 is the permeability of a vacuum, and r_{12} is the distance between the charges.

A field strength E is the electrostatic force produced per unit charge of the particle. This field is then

$$E = \frac{F_e}{q_p} \quad (118)$$

where $q_p = ne$, n being the number or units of electron charge, e is 1.6×10^{-19} Coulombs.

The work required to move a particle distance 'x' in an electric field per unit charge is

$$W_p = \frac{F_e \Delta x}{q_p} \quad (119)$$

This work is the potential difference in the electric field and is measured in volts, e.g., the voltage between parallel plates in an electrostatic precipitator.

The difference between the drag force and the electrostatic force determines particle acceleration in an electric field

$$F_e - F_d = m_p \frac{dv_p}{dt} \quad (120)$$

6.2.3 Particle Motion Induced by Temperature Gradients

A temperature gradient will result in particles moving from the warmer region to the cooler region or surface. This phenomenon is the result of thermophoretic forces on the particles.

6.2.3.1 Thermophoretic Motion for Gases and Particles with Diameter Less Than the Molecular Mean Free Path

When the Knudsen number, $Kn = \lambda/d_p$, is greater than 1.0, the thermophoretic velocity is given by

$$V_{\text{Thermo}} = -0.55 \frac{\mu}{\rho T} \nabla T \quad (121)$$

where $\nabla T = \frac{T_{\text{hot}} - T_{\text{cold}}}{ds}$ and T is the ambient or bulk temperature of the fluid (Hinds, 1982).

6.2.3.2 Thermophoretic Transport for Particles with Diameter Greater Than the Molecular Mean Free Path

When $Kn < 1.0$, the particle is influencing inertial and thermodynamic states of nearby gas molecules. The thermophoretic velocity is found by equating resistive forces to the thermal force (Hinds, 1982) and is given by

$$V_{\text{Thermo}} = -\frac{3}{2} H \frac{\mu}{\rho T} \nabla T C_c \quad (122)$$

where T is the ambient or bulk temperature of the fluid, C_c is the Cunningham slip correction factor, and

$$H = \left[\frac{1}{1 + 6\lambda/d_p} \right] \left[\frac{\frac{k_f}{k_p} + 4.4\lambda/d_p}{1 + 2\frac{k_f}{k_p} + 8.8\lambda/d_p} \right] \quad (123)$$

where k_f and k_p are the thermal conduction of the fluid and particle, respectively.

Thermophoretic forces have an insignificant influence on the rate of deposition for particles of one micron physical diameter or larger. For very small particles, this velocity would add as a vector function to the settling velocity and the velocity of the air stream.

6.3 Particle Flow in Inlets and Flanges

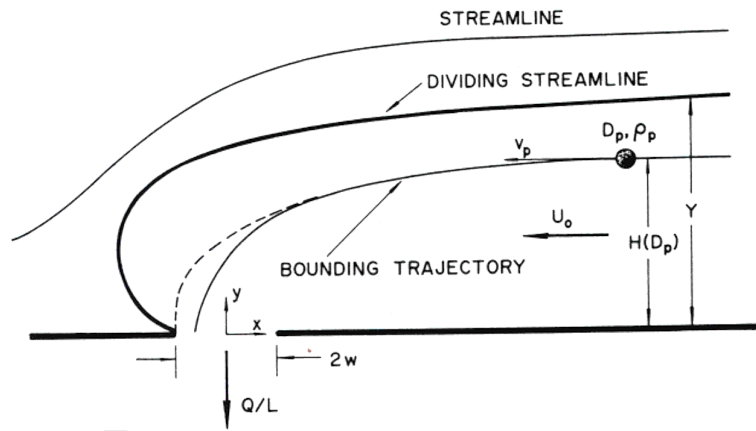
Contaminants and air are withdrawn by inlets of various shapes and sizes. The effectiveness of an inlet is basically how well it serves to capture contaminants. The locations of dividing streamlines and bounding trajectories of particles can be determined as a first guess using much of the analytical tools previously discussed. The quantitative measure of inlet effectiveness is generally referred to as *reach*. The reach defines the boundaries of the region from which the inlet reaches out and captures contaminants. In more definable terms, the reach can be defined as the ratio of the cross-sectional area of the stream tube of contaminants entering the inlet to the cross-sectional area of the stream tube of air entering the

inlet. The reach for particles is not always equal to one since some of the particles may not enter the inlet, even though all the air is pulled into the inlet. This is due to particle inertia and deflection. For gases and vapors, the reach is unity. Figure 9 (a-d) shows a set of dividing streamlines and bounding trajectories for several flanged inlet configurations.

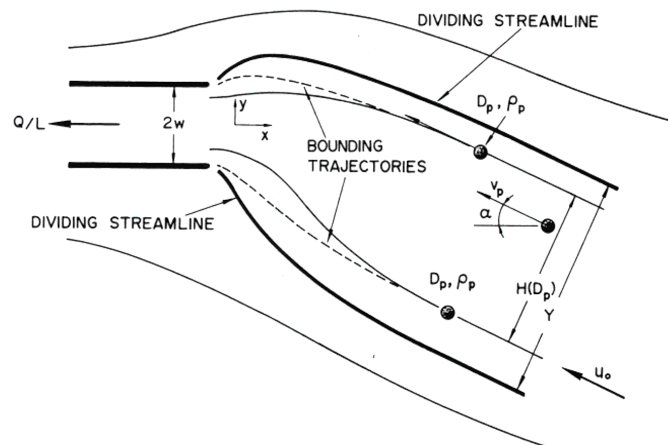
To find particle velocity, displacement, and its new location (x, y) , Equation (108) must first be solved. Once the velocities are determined, the location of the particle at the end of an interval of time can be found using the simple relations

$$\begin{aligned}x_j &= x_i + \Delta t u(x_i, y_i) \\y_j &= y_i + \Delta t v(x_i, y_i)\end{aligned}\quad (124)$$

where i denotes initial (previous) position and j is the new position. Repeating solution of this pair of equations produces a table of x and y values that can be used to create a trajectory for the particle position. More details on this simple technique are given later in the section on Lagrangian Particle Transport.



(a)



(b)

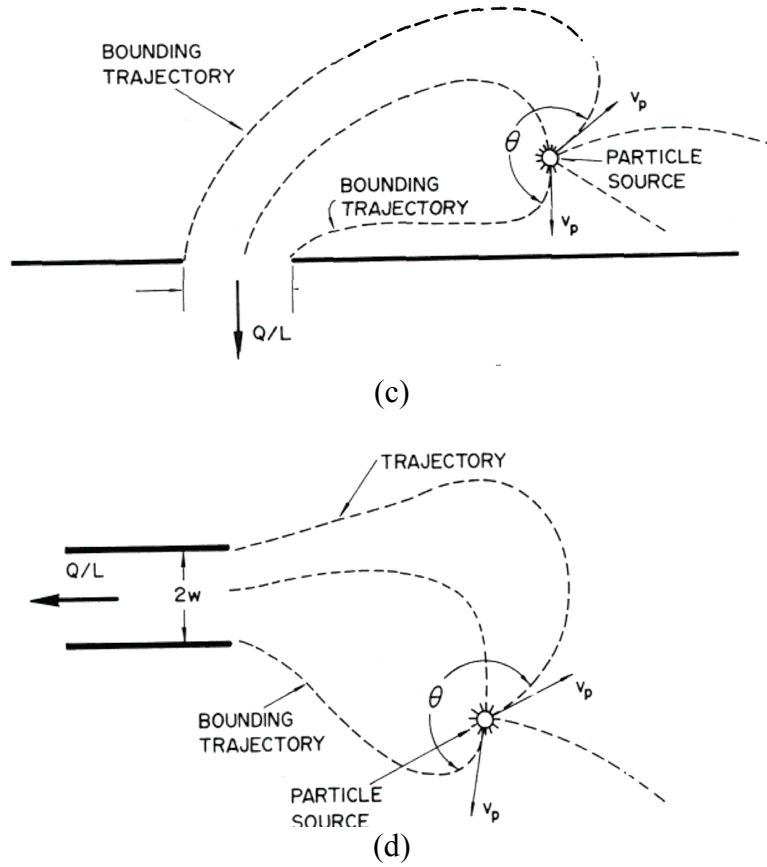


Figure 9. Dividing streamline and bounding trajectory for flanged inlets (from *Industrial Ventilation*, R. J. Heinsohn, J. Wiley & Sons, New York, 1991, pg. 518).

Figure 10 shows the dividing streamlines and bounding trajectories for particles of varying sizes entering an unflanged inlet.

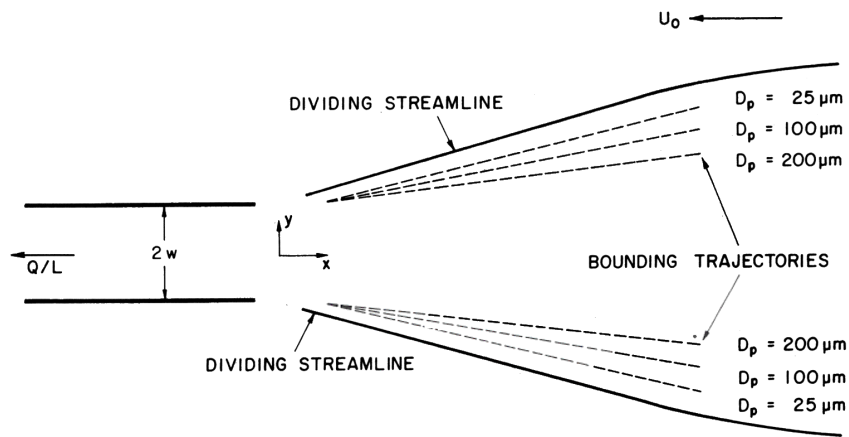


Figure 10. Reach of an unflanged inlet for several particle sizes (from *Industrial Ventilation*, R. J. Heinsohn, J. Wiley & Sons, New York, 1991, pg. 537).

7 Numerical Modeling - CFD

Indoor air quality can have a larger effect on human health than outdoor air quality. The common practice of relating measurements of outdoor pollutants to human exposure can be fundamentally wrong, especially with regards to hazardous material. Direct measurements of indoor air quality are the best way to evaluate the existence and the gravity of contaminants. In some instances, statistical data can be used to estimate flow rates. While such analyses lead to order of magnitude projections, they do not provide sufficient data for ventilation feedback and remediation. In order to obtain accurate assessments and forecasts of the effects on ventilation/air quality, modeling based on solution of the nonlinear equations of fluid motion (CFD) must be undertaken.

There are four fundamental numerical methods that are currently being used to model flow and species transport within enclosures. The two most popular and most prevalent methods are numerical models that utilize finite difference and finite volume techniques.

7.1 Finite Difference Method

Representing a derivative using a Taylor series and truncating higher order terms creates an approximation to that derivative. In this manner, when discrete distances and increments of time are employed in the Taylor series expansion, a finite difference approximation is made of the original differential equation. For example, looking at the 1-D equation for time dependent isotropic advection-diffusion,

$$\frac{d\phi}{dt} + u \frac{\partial\phi}{\partial x} = k \frac{\partial^2\phi}{\partial x^2} \quad (125)$$

we seek the derivatives of each term, found by Taylor series expansion.

Representing the derivative of f with respect to x we have

$$\phi_{x+1} = \phi_x + \frac{\partial\phi}{\partial x} \Delta x + \frac{1}{2!} \frac{\partial^2\phi}{\partial x^2} \Delta x^2 + \dots \quad (126)$$

Rearranging and dropping higher order terms, the first order derivative is represented in a discrete sense as

$$\frac{\partial\phi}{\partial x} = \frac{\phi_x - \phi_{x-1}}{\Delta x} \quad (127)$$

where a backward difference method is used.

Adding both the forward and backward Taylor series, the second order discrete derivative is

$$\frac{\partial^2 \phi}{\partial x^2} = \frac{\phi_{x+1} - 2\phi_x - \phi_{x-1}}{\Delta x^2} \quad (128)$$

Substituting these and the discrete time advancement

$$\frac{\partial \phi}{\partial t} = \frac{\phi_x^{t+1} - \phi_x^t}{\Delta t} \quad (129)$$

into the advection-diffusion equation results in the discrete representation of the governing equation

$$\frac{\phi_x^{t+1} - \phi_x^t}{\Delta t} + u \frac{\phi_x - \phi_{x-1}}{\Delta x} = k \frac{\phi_{x+1} - 2\phi_x - \phi_{x-1}}{\Delta x^2} \quad (130)$$

This equation is first order, accurate in time and space, although the diffusion term is second order accurate. Higher order discretization can be achieved with the use of various components of the Taylor series expansions. Also, notice this equation was developed based on an equal spacing of the discretization and could be modified for non-uniform grid spacing.

If this equation had been in 2-D, it would be apparent that the discretization had an orthogonality, the x and y discretization were perpendicular. This decomposition of the domain into grid points that can be connected by lines orthogonal is referred to as a structured grid. For complex domains the representation may suffer if there are curved surfaces or sides oblique to the discretization. Transformations can be constructed for complex domains that fit the complex boundaries and coordinates to an orthogonal discretization. This Boundary Fitted Coordinate (BFC) transformation can be complex but allows for the use of both FDM and structured FVM to solve problems on complex domains (Fletcher, 1991).

Upwinding of the advective term, i.e., a backward differencing, is employed since it is a stable discretization even for explicit time stepping. The stability constraint is the Courant-Friedrichs-Lewy (CFL) condition

$$C = u \frac{\Delta t}{\Delta x} \leq 1 \quad (131)$$

The condition states that a fluid molecule can travel no more than a spatial distance Δx in time Δt . It is interesting to write the upwinded term with a

numerical diffusion, thus indicating a damping of the 2nd order central difference scheme.

$$\frac{u}{\Delta x}(\phi_x - \phi_{x-1}) = \frac{u}{2\Delta x}(\phi_{x+1} - \phi_{x-1}) - \frac{u}{2\Delta x}(\phi_{x+1} - 2\phi_x + \phi_{x-1}) \quad (132)$$

This dampening is advantageous in capturing step gradients common to the advective term, the wave equation portion of the advection-diffusion model, as is indicated by its more stable nature (Fletcher, 1994).

Time advancement is accomplished either by implicit, semi-implicit or explicit formulation of the equation. When all the nodal values in each equation are being solved at the next time step, it is an implicit formulation. This formulation has no limiting value for the time increment (i.e., it is unconditionally stable).

Placing only the node being evaluated for time advancement in each equation on the left hand side (LHS) produces an explicit formulation. An explicit formulation's time increment is constrained by the CFL condition and also by diffusion, by the Fourier number

$$k \frac{\Delta t}{\Delta x^2} \leq \frac{1}{2} \quad (133)$$

Using a scheme, which averages in space the current and future time step is known as a semi-implicit scheme, the Crank-Nicholson averaging process, and is conditionally stable. Numerous other time marching schemes have been devised. An alternating direction implicit (ADI) scheme is particularly useful in separating multi-dimensional systems into time advancement for each dimension and is conditionally stable for this equation set.

7.2 Finite Volume Method

The majority of fluid flow simulations have been conducted using the finite volume approach (Patankar, 1980; Anderson et al., 1984), principally because of its ease of use and simplicity in establishing meshes for orthogonal regions (i.e., rectangles). Introduction of the Boundary Fitted Coordinates (BFC) technique to model irregular geometries helped in overcoming this handicap (Thompson et al., 1985). However, the computational accuracy of these simple difference schemes is limited to first order (spatially); in addition, such methods require extensive meshing effort and massive numbers of nodes (especially in three dimensions), and can become quite formidable for non-orthogonal problem domains. Modeling 3-D problems using finite volume (or finite difference) methods may typically require over 10^6 nodes, overwhelming the resources of the largest supercomputers.

Finite volume method (FVM) is a subset of the Method of Weighted Residuals (MWR) and in this sense is a cousin to the finite element method (FEM). It is an inner product projecting the residual to zero. Since the problem domain is a discrete system, the method seeks to minimize the error or residual, R , over the domain. Let the residual equation or relationship be determined by

$$R(L(\hat{u})) \quad (134)$$

where $L(\hat{u})$ is the approximation to any or some differential equation $L(u)$. The approximation of the function \hat{u} is given by

$$\hat{u}(x_i) = \sum_{i=1}^n u_i N_i \quad (135)$$

which is a polynomial expansion. The term N_i is the weight and \hat{u}_i is the trial value. For the FVM, this weight is just one or zero depending on if the elemental domain is being evaluated or not, and n is equal to 1.

The method seeks to minimize this residual over a domain. Requiring the residual to be zero on average is accomplished by multiplying the residual equation by the appropriate weighting function, w , and integrating over the entire domain

$$\int_{\Omega} w R(L(\hat{u})) d\Omega = 0 \quad (136)$$

When applied over a domain, which is discretized into finite volumes, the resulting set of algebraic equations can be solved for the unknowns, that is, the values of \hat{u} ,

$$\int_{\Omega} (R, w) d\Omega = 0 \quad (137)$$

where the residual R is the approximate solution and w is some appropriate weight or approximation. The residual is by definition approximate since only an approximation of the solution on the domain is possible with any discrete representation. It is possible however, to have an exact solution at the nodal points, known as superconvergence.

The difference between FEM and FVM is in the order of the interpolation polynomial where FEM has at least first order weighting functions and the variables are also represented as functions of higher order polynomials. The finite volume method uses zero order polynomials as both test and weight functions. The finite volume method is referred to as a subdomain method. To see how this works, we look at the equation for conservation of mass in integral form

$$L(u) = \nabla \cdot \rho \hat{v} = 0 \quad (138)$$

then

$$\int_{\Omega} L(u) \, d\Omega = \int_{\Omega} \nabla \cdot \rho \hat{v} \, d\Omega \quad (139)$$

Applying Green's Theorem, we have

$$\int_{\Omega} \nabla \cdot \rho \hat{v} \, d\Omega = \oint_{\Gamma} (\hat{n} \cdot \rho \hat{v}) \, d\Gamma \quad (140)$$

This integral equation evaluated over the domain Ω (shown in Figure 11) produces an expression for the conservation of mass given by

$$\rho_r u_r A_r - \rho_l u_l A_l + \rho_t u_t A_t - \rho_b u_b A_b = 0 \quad (141)$$

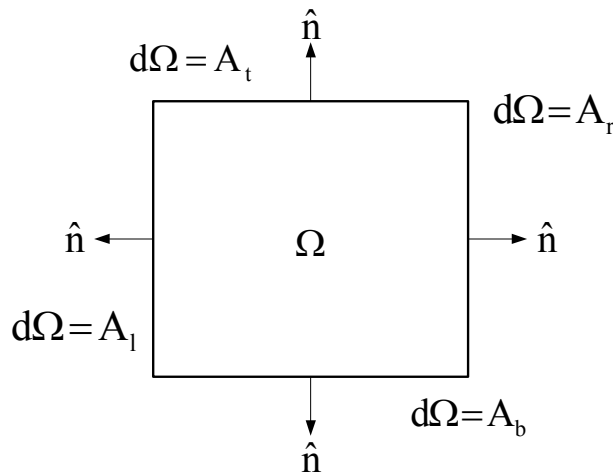


Figure 11. A finite volume.

If we assign and assume the values of ρ at the center of the cells, the values of velocity at the faces of each cell, an offset grid is created which avoids the difficulties associated with $2\Delta x$ instabilities (Hansen, 1996). This discretization is shown in Figure 12.

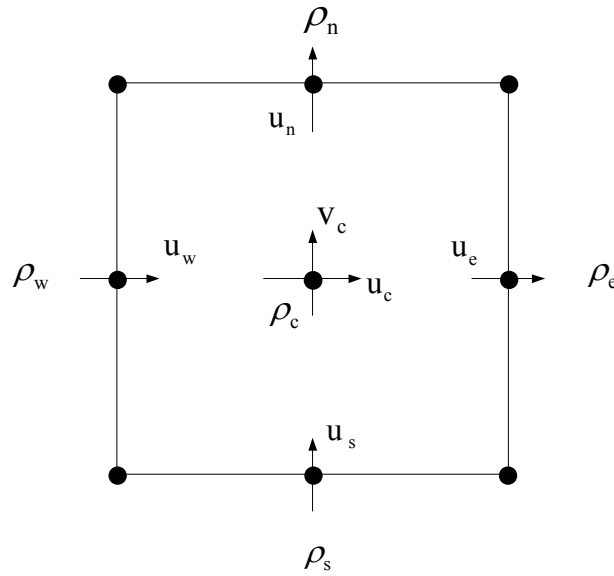


Figure 12. Discretization of a finite volume.

To avoid discretizations that might not have any physical meaning, an upwinding scheme is used. Only the center density belongs to the cell and is considered constant throughout the cell. Therefore ρ_w, ρ_e, ρ_s and ρ_n belong to the adjacent cells and are evaluated at the center of those cells. However, the velocities do belong to the points depicted on the faces of the cell. Upwinding is accomplished as follows

$$(\rho u)_e = \rho_c \text{Max}(u_c, 0) - \rho_e \text{Max}(-u_e, 0) \quad (142)$$

Noticing from Figure 12 that

$$\begin{aligned} A_t &= A_b = \Delta y \\ A_e &= A_w = \Delta x \end{aligned} \quad (143)$$

the discretized equation for mass conservation becomes

$$\int_{\Omega} \nabla \cdot \rho \hat{v} \, d\Omega \equiv \oint_{\Gamma} (\hat{n} \cdot \rho \hat{v}) \, d\Gamma \cong [(\rho u)_e - (\rho u)_w] \Delta y + [(\rho u)_n - (\rho u)_s] \Delta x \quad (144)$$

The momentum equations are developed similarly. If the elements are trapezoidal (2-D) or hexahedral (3-D), the surface areas and normal dot products must be calculated in order to evaluate the correct flux, thereby rendering this system capable of handling a non-orthogonal grid discretization.

7.3 The Finite Element Method

A numerical method that is capable of handling the wide variety of complex problems inherent in today's technology is the finite element method (Zienkiewicz, 1977). The reasons for its popularity include the ability to handle inhomogeneous or variable properties, irregular boundaries, and use of general-purpose algorithms that give high order accuracy. However, traditional finite element methods are not without their faults. The computational effort and storage requirements associated with traditional finite element methods rapidly become excessive when solving fluid flow problems. The bandwidth generated from the computational mesh and assembly procedure is critical when globally formulating the coefficient matrices. Problems involving a large number of nodes become difficult to solve on even the largest and fastest computers. Pepper (1987) and Pepper and Singer (1990) discuss accurate finite element algorithms that are computationally efficient, and are particularly advantageous in modeling large problems on small computers.

Bilinear isoperimetric quadrilateral elements are used to discretize 2-D problem domains; trilinear hexahedral elements are used for 3-D domains. The standard weak formulation of the Galerkin weighted residual technique is employed to cast Equations (1)-(6) into their integral form.

Conservation of Mass

$$\int_{\Omega} \left(\frac{\partial u}{\partial x} + \frac{\partial v}{\partial y} + \frac{\partial w}{\partial z} \right) W_i \, d\Omega = 0 \quad (145)$$

Conservation of Momentum

x-direction

$$\int_{\Omega} \left[\rho \left(\frac{\partial u}{\partial t} + u \frac{\partial u}{\partial x} + v \frac{\partial u}{\partial y} + w \frac{\partial u}{\partial z} \right) + \frac{\partial p}{\partial x} - \frac{\partial \sigma_{xx}}{\partial x} - \frac{\partial \sigma_{xy}}{\partial y} - \frac{\partial \sigma_{xz}}{\partial z} - f_x \right] W_i \, d\Omega = 0 \quad (146)$$

y-direction

$$\int_{\Omega} \left[\rho \left(\frac{\partial v}{\partial t} + u \frac{\partial v}{\partial x} + v \frac{\partial v}{\partial y} + w \frac{\partial v}{\partial z} \right) + \frac{\partial p}{\partial y} - \frac{\partial \sigma_{yx}}{\partial x} - \frac{\partial \sigma_{yy}}{\partial y} - \frac{\partial \sigma_{yz}}{\partial z} - f_y \right] W_i \, d\Omega = 0 \quad (147)$$

z-direction

$$\int_{\Omega} \left[\rho \left(\frac{\partial w}{\partial t} + u \frac{\partial w}{\partial x} + v \frac{\partial w}{\partial y} + w \frac{\partial w}{\partial z} \right) + \frac{\partial p}{\partial z} - \frac{\partial \sigma_{zx}}{\partial x} - \frac{\partial \sigma_{zy}}{\partial y} - \frac{\partial \sigma_{zz}}{\partial z} - f_z \right] W_i \, d\Omega = 0 \quad (148)$$

Conservation of Energy

$$\int_{\Omega} [\rho c_p \left(\frac{\partial T}{\partial t} + u \frac{\partial T}{\partial x} + v \frac{\partial T}{\partial y} + w \frac{\partial T}{\partial z} \right) - \frac{\partial q_x}{\partial x} - \frac{\partial q_y}{\partial y} - \frac{\partial q_z}{\partial z} - Q] W_i d\Omega = 0 \quad (149)$$

Species Concentration

$$\begin{aligned} & \int_{\Omega} \left[\frac{\partial C}{\partial t} + u \frac{\partial C}{\partial x} + v \frac{\partial C}{\partial y} + w \frac{\partial C}{\partial z} \right] W_i d\Omega + \\ & \int_{\Omega} \left[-\frac{\partial}{\partial x} \left(D_{xx} \frac{\partial C}{\partial x} \right) - \frac{\partial}{\partial y} \left(D_{yy} \frac{\partial C}{\partial y} \right) - \frac{\partial}{\partial z} \left(D_{zz} \frac{\partial C}{\partial z} \right) - S \right] W_i d\Omega = 0 \end{aligned} \quad (150)$$

where Ω denotes the computational domain and W_i is the weighting function. The u , v , w , p , T , and C variables are represented by the trial approximations

$$\begin{aligned} u(x, y, z, t) &= \sum N_i(x, y, z) \hat{u}(t) \\ v(x, y, z, t) &= \sum N_i(x, y, z) \hat{v}(t) \\ &\text{etc.} \end{aligned} \quad (151)$$

where N_i is the basis function; in this instance, $W_i = N_i$. The matrix equivalent formulations of Equation (152) are written as

$$\begin{aligned} C^T \vec{V} &= 0 \\ M \dot{\hat{u}} + [K + A(\vec{V})] \hat{u} + C^x p &= F_u \\ M \dot{\hat{v}} + [K + A(\vec{V})] \hat{v} + C^y p &= F_v \\ M \dot{\hat{w}} + [K + A(\vec{V})] \hat{w} + C^z p &= F_w \\ M \dot{\hat{T}} + [K + A(\vec{V})] \hat{T} &= F_T \\ M \dot{\hat{C}} + [K + A(\vec{V})] \hat{C} &= F_C \end{aligned} \quad (152)$$

where the $\dot{\cdot}$ refers to time differentiation, \wedge denotes trial function, and V is the velocity vector. The matrix coefficients are traditionally defined (using the Green-Gauss theorem)

$$\begin{aligned}
\mathbf{K} &= \int_{\Omega} \left(\frac{\partial N_i}{\partial x} \frac{\partial N_j}{\partial x} + \frac{\partial N_i}{\partial y} \frac{\partial N_j}{\partial y} + \frac{\partial N_i}{\partial z} \frac{\partial N_j}{\partial z} \right) d\Omega \\
\mathbf{A}(\vec{\mathbf{V}}) &= \int_{\Omega} \left(u_k N_k N_i \frac{\partial N_j}{\partial x} + v_k N_k N_i \frac{\partial N_j}{\partial y} + w_k N_k N_i \frac{\partial N_j}{\partial z} \right) d\Omega \\
\mathbf{C}^x &= \int_{\Omega} N_i \frac{\partial N_j}{\partial x} d\Omega, \quad \mathbf{C}^y = \int_{\Omega} N_i \frac{\partial N_j}{\partial y} d\Omega, \quad \mathbf{C}^z = \int_{\Omega} N_i \frac{\partial N_j}{\partial z} d\Omega \\
\mathbf{C}^T &= \begin{Bmatrix} \mathbf{C}^x \\ \mathbf{C}^y \\ \mathbf{C}^z \end{Bmatrix}
\end{aligned} \tag{153}$$

$$\begin{aligned}
\mathbf{F}_u &= \int_{\Gamma_u} N_i \left(\frac{\partial u}{\partial x} \hat{n}_x + \frac{\partial u}{\partial y} \hat{n}_y + \frac{\partial u}{\partial z} \hat{n}_z \right) d\Gamma_u \\
\mathbf{F}_v &= \int_{\Gamma_v} N_i \left(\frac{\partial v}{\partial x} \hat{n}_x + \frac{\partial v}{\partial y} \hat{n}_y + \frac{\partial v}{\partial z} \hat{n}_z \right) d\Gamma_v \\
\mathbf{F}_w &= \int_{\Gamma_w} N_i \left(\frac{\partial w}{\partial x} \hat{n}_x + \frac{\partial w}{\partial y} \hat{n}_y + \frac{\partial w}{\partial z} \hat{n}_z \right) d\Gamma_w \\
\mathbf{F}_T &= \int_{\Gamma_T} \kappa N_i \left(\frac{\partial T}{\partial x} \hat{n}_x + \frac{\partial T}{\partial y} \hat{n}_y + \frac{\partial T}{\partial z} \hat{n}_z \right) d\Gamma_T \\
\mathbf{F}_C &= \int_{\Gamma_C} N_i \left(K_{xx} \frac{\partial C}{\partial x} \hat{n}_x + K_{yy} \frac{\partial C}{\partial y} \hat{n}_y + K_{zz} \frac{\partial C}{\partial z} \hat{n}_z \right) d\Gamma_C
\end{aligned} \tag{154}$$

where the i , j , and k subscripts denote summation over the local nodes within an element and $d\Gamma_u$, $d\Gamma_v$, $d\Gamma_w$, $d\Gamma_T$, and $d\Gamma_C$ represent boundary segments over which gradients of u , v , w , T , and C are specified.

The use of classical finite element methods to solve fluid flow problems generally requires large amounts of computational storage. The bandwidth generated as a result of the computational mesh and assembly procedures in formulating the coefficient matrices are critical. In addition, classical finite element methods tend to be slower in execution (but not necessarily in convergence to steady state) than finite difference methods as a result of repeated matrix multiplications and global assembly. Equations (153)-(154) are evaluated using Gaussian quadrature with 2 x 2 (2-D quadrilateral) or 2 x 2 x 2 (3-D hexahedral) Gauss points, and the overall global matrix solved via some form of Gaussian elimination. Figure 13 shows the 2-D (four node) and the 3-D (eight node) generic elements.

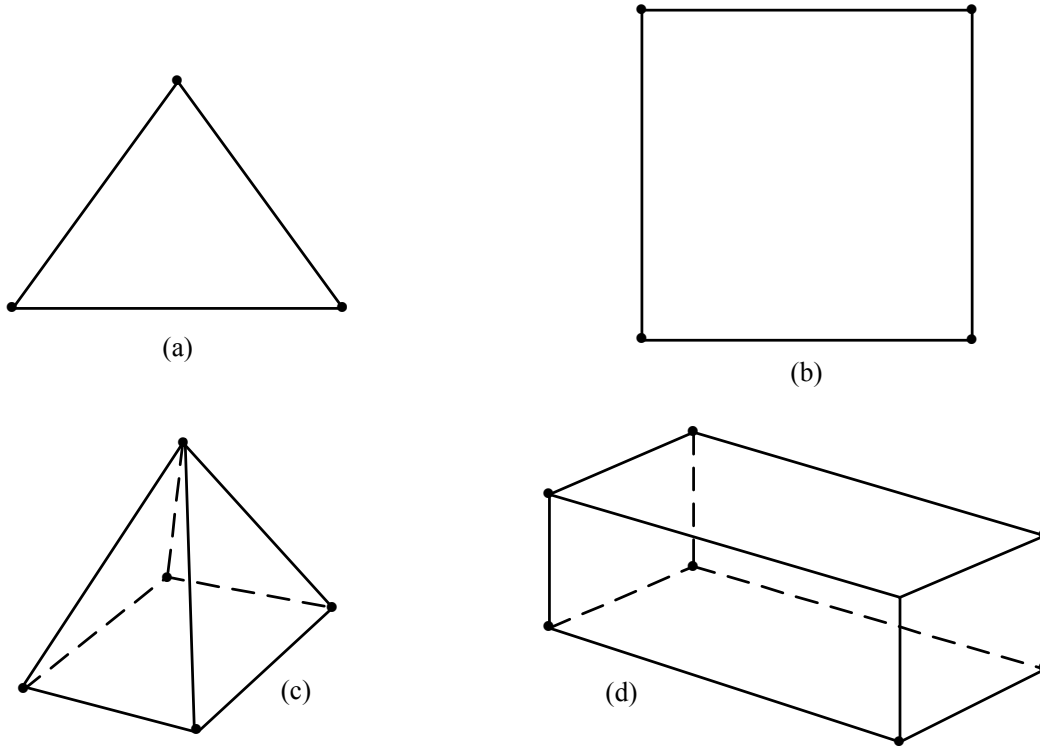


Figure 13. Generic finite elements: (a) 3 node triangle, (b) 4 node bilinear, (c) 5 node tetrahedral, (d) 8 node hexahedral.

7.3.1 Petrov-Galerkin

The Petrov-Galerkin formulation is obtained by perturbing the weighting for the advection term (only) such that

$$W_i = N_i + \frac{\alpha h_e}{2V} \left(u \frac{\partial N_i}{\partial x} + v \frac{\partial N_i}{\partial y} + w \frac{\partial N_i}{\partial z} \right) \quad (155)$$

where h_e is the element size, and α is defined as (Yu and Heinrich, 1986)

$$\alpha = \coth \frac{\beta}{2} - \frac{2}{\beta} \quad (156)$$

with $\beta = |V|h_e R_e / 2$, which is the cell Reynolds number. The use of this weighting function is particularly attractive when coupled with adaptive meshing.

The pressure is obtained from the "discrete" momentum equations and a time-difference version of the continuity equation. An explicit forward-in-time Euler scheme is used to advance the discretized equations in time.

7.4 Mesh Adaptation

Adaptive gridding methods concentrate computational cells in regions where the solution is rapidly changing and leave the grid coarse in regions where the solution is smooth. Because of the tremendous potential adaptive gridding has for reducing computational costs while maintaining the same level of accuracy, it is a forefront area in computational physics. Adaptation can occur within any element shape, i.e., triangles or quadrilaterals, tetrahedrals or hexahedrals (Pelletier and Ilinca, 1994; Pepper and Emery, 1994).

It is often necessary to resolve discontinuities or localized steep gradients in the computational domain; however, the cost of using enough closely spaced zones to resolve those regions as they move throughout the entire computational domain is high. Furthermore, such fine resolution is of no benefit in most of the domain. In these cases, adaptive gridding algorithms are used in which small computational cells are placed only in those regions with large gradients.

Refined localized gridding techniques for boundary layers in steady state calculations have been used for years. For many transient fluid problems with a fixed but complicated boundary geometry, adaptive gridding is used to obtain accurate answers with a modest number of grid points. These problems arise, for example, within interior flows and in external aerodynamics.

In the simplest application of adaptive gridding, equally spaced elements are established initially at the beginning of the calculation (see Figure 14, a-c). They are then adapted in time to the domain boundaries and to average properties of the flow. As the regions in the flow requiring the most accuracy become localized, the elements move relative to the localization, i.e., the gridding algorithm changes the mesh in the course of the calculation to keep the resolution localized where it is needed.

The criterion for clustering closely spaced elements is related to a local variable, such as velocity, temperature, or species concentration. The change in the variables, their derivatives, and their curvatures may be estimated to determine whether more or less resolution is needed, and the cell spacing can be adjusted (or divided as in Figure 14) to minimize the overall error.

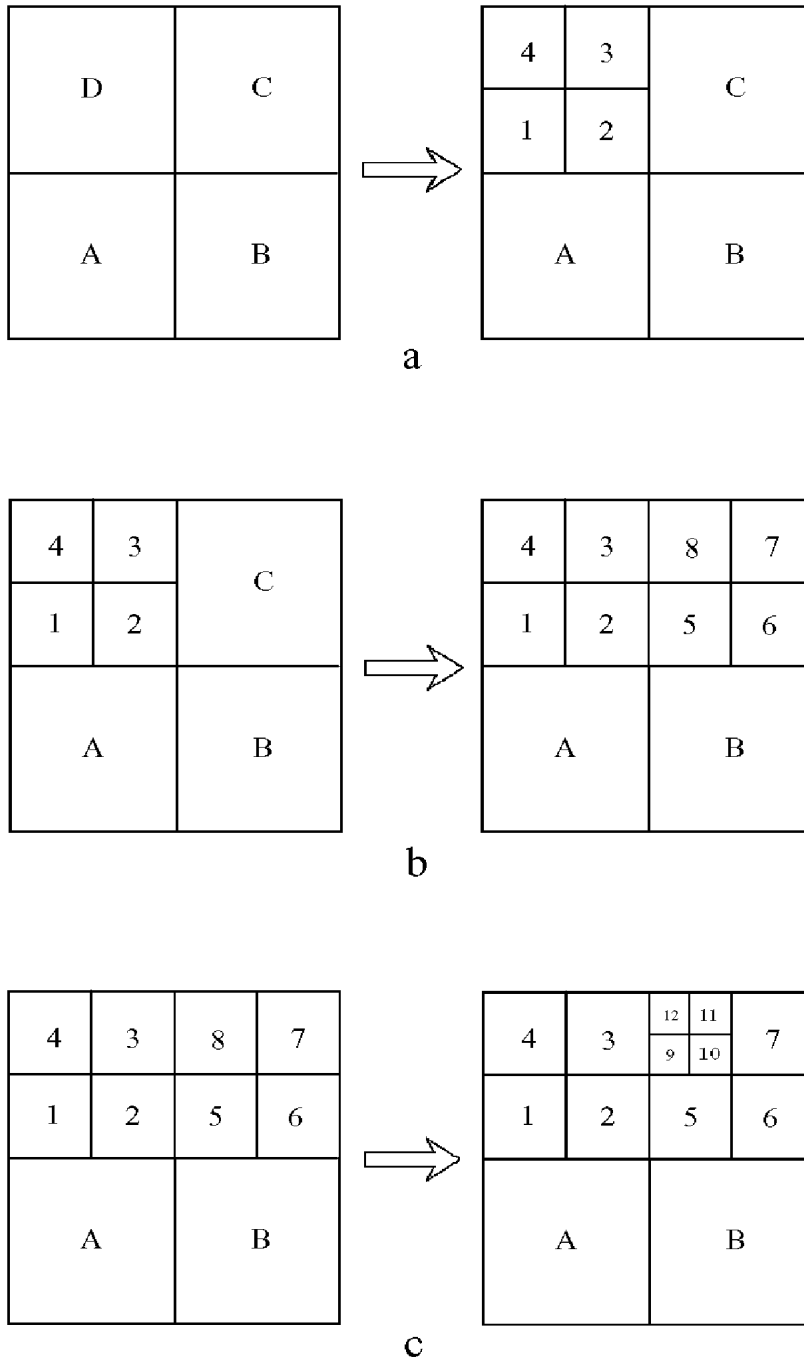


Figure 14. 2-D adaptive sequence.

7.5 Boundary Conditions for Mass Transport Analysis

Gas and particulate flux boundary conditions are of the form

$$q_{p_j} = h_{p_j} (C_{j \text{ at boundary}} - C_{\text{bluk}_j}) \quad (157)$$

where q_{p_j} is the flux rate of the j^{th} particle or substance, C_{bulk_j} is a bulk concentration in the fluid stream, and a boundary concentration $C_{j \text{ at boundary}}$ is just at the boundary.

Such an equation is basic; it is Newton's law of cooling applied to mass. The statement is general and is true for any substance. It is merely stating that the rate of transfer per unit area is the difference in concentration between one place and another multiplied by some constant. Only the convective coefficient h_{p_j} needs determining.

The convective coefficient h_{p_j} in the boundary condition above is determined by geometry, electrostatic forces, gravity, other forces affecting particulate inertia, diffusivities, partial pressures of vapors, chemical bonding, etc.

Another way of formulating the flux term for a strictly diffusion related flux is

$$J_j = D_j \nabla C_j \quad (158)$$

This is Fick's first law of diffusion (Reist, 1993) where J_i is mass flux and in one dimension.

Both forms of boundary conditions have units of mass per unit time per unit area. Different formulations are required as the significance of the forces acting on the mass changes and the type of mass in consideration. For an evaporating liquid, the first form is typically employed. For particulate depositing to a surface, or gases migrating without phase change at the boundary, the second form is more appropriate as it directly incorporates the diffusion coefficient. Particles with one-micron aerodynamic diameter or less do not experience gravitational settling or significant relaxation times. Therefore, a division at one-micron makes a natural delineation between the behavior of larger and smaller particles.

Diffusion, thermophoretic forces, and particle agglomeration (with associated increase in settling velocity) are responsible for deposition. For small particles, a settling velocity is essentially nonexistent. In the absence of inertial, thermophoretic forces and other forces, molecular diffusion through a boundary layer is responsible for most deposition of particles smaller than one micron.

If an analytic boundary layer solution were to be obtained, a deposition velocity could be calculated. The deposition velocity is given by the following diffusion velocity

$$V_d = \frac{\text{Rate of Deposition}}{C_{bulk} - C_{wall+}} \quad (159)$$

and for a concentration at the boundary or wall which is not affecting the rate of deposition (Davies, 1966)

$$V_d = \frac{J_j}{C_{\text{bulk}_j}} \quad (160)$$

For purely diffusive deposition, substituting for $\frac{dC_j}{dx} = \frac{C_{\text{boundary}} - C_{\text{bulk}_j}}{\delta_{p_j}}$, where dx is a boundary thickness over which there is a change in concentration, then

$$V_d = \frac{D_j}{\delta_{p_j}} \quad (161)$$

where V_d is deposition velocity and δ_{p_j} is a boundary layer thickness for the j^{th} particulate. This equation is for the case of sedimentation where the surface concentration is unimportant to the flow (Davies, 1966).

Rate of deposition is not affected by the flow. The difficulty with this equation is the determination of the boundary layer thickness, δ_{p_j} . It is essentially defined as the distance at which the gradient of concentration is zero. The bulk concentration is a function of distance changing in time as material is deposited from the flow.

Deposition of particulate in the numerical model is treated as a flux boundary. The mass flux to the wall has a value of the deposition equal to the deposition velocity. The mechanism for deposition is Fickian diffusion in the absence of other influencing forces. Deposition of inert gases onto a surface is zero. Other gases deposit via some reaction mechanisms for which rates must be specified. For deposition other than by diffusion, rates are generally determined experimentally.

Turbulence provides good mixing; therefore, if a homogenous concentration everywhere beyond the diffusive boundary layer is assumed, the deposition velocity becomes

$$V_d = \frac{\text{Rate of Deposition}}{C_\infty - C_0} = \frac{D_j}{\delta_{p_j}} \quad (162)$$

The difficulty again lies with the determination of δ_{p_j} .

The rate of transport in turbulent flow of a substance towards a surface in nondimensional form is (Davies, 1966)

$$\frac{R}{u_* c_o} = \left(\frac{D_j + \mu_{\text{turb}}}{v_{\text{fluid}}} \right) \frac{dc_+}{dy_+} \quad (163)$$

where:

$c_+ = c / c_o$ is nondimensional concentration at any given time

$y_+ = y u_* / v_{\text{fluid}}$ is nondimensional distance normal to a surface

$V_d = R / c_o$ is the deposition velocity

$u_* = \sqrt{\frac{\tau_w}{\rho_f}}$ is the friction velocity

By substituting these terms, an expression for the nondimensional V_+ is found as

$$\frac{V_+}{u_*} = \left(\frac{D_j + \mu_{\text{turb}}}{v_f} \right) \frac{dc_+}{dy_+} \quad (164)$$

The diffusive term is a linear combination of the turbulent eddy diffusivity μ_{turb} , and Fickian diffusivity, D_j . The deposition velocity is derived from the nondimensional deposition velocity by $V_+ = V_d / u_*$, where u_* is the friction velocity.

As previously mentioned, a numerical model for deposition of particulate is essentially treated as a flux boundary. The mechanism for deposition is Fickian diffusion only through the laminar sublayer. The mechanism for distribution into the turbulent sublayers is by turbulent diffusion. Unless a concentration is specified on the surface, the law of the wall is not necessary for calculation of the mass gradient.

7.6 Boundary Element Method

The boundary element method is a unique numerical scheme, which permits rapid and accurate solution of a specific class of equations (Brebbia and Dominguez, 1989). Employing Green's identity, the boundary element method (BEM) requires only the discretization of the boundary domain - no internal mesh is required as in the finite element method. The BEM reduces the dimensionality of a problem by one (i.e., a two-dimensional problem reduces to a line integral); a three-dimensional problem reduces to a two-dimensional surface formulation. Hence, input data processing consists only of the boundary geometry and boundary condition problem. The governing equation for advection-diffusion utilizing a scalar potential, ϕ , can be written as

$$L[\phi] \equiv \frac{\partial \phi}{\partial t} + \nabla \cdot (-k \nabla \phi) + (V \cdot \nabla) \phi - S \quad (165)$$

where V is the velocity vector, k is the dispersivity tensor, t is time, and S denotes the source density. Assuming steady-state, the governing operator $L[\phi]$ and its adjoint operator $L^*[\psi]$, in which ψ is the adjoint potential associated with ϕ to Green's second identity, can be written as

$$\int_{\Omega} (L[\phi]\psi - L^*[\psi]\phi) d\Omega = \int_{\Gamma} k \left(\phi \frac{\partial \psi}{\partial n} - \frac{\partial \phi}{\partial n} \psi \right) d\Gamma + \int_{\Gamma} V_n \phi \psi d\Gamma \quad (166)$$

where n is the outward normal to ϕ , and V_n is the normal component of V to Γ . If one introduces the fundamental solution ψ^* of $L^*[\psi] = 0$ instead of ϕ , Equation (166) can be rewritten as

$$c_i \phi(r_i) - \int_{\Gamma} q_n^* \phi d\Gamma = - \int_{\Gamma} \psi^* q_n d\Gamma + \int_{\Omega} S \psi^* \quad (167)$$

where c_i denotes a coefficient that depends on the position vector r_i , $q_n^* = n(-k \nabla \psi^* - V \psi^*)$, $q_n = n(-k \nabla \phi)$ and ψ^* is

$$\psi^*(r; r_i) = \exp\{-(V \cdot r' + |V| |r'|)/(2K)\} / (4\pi K |r'|) \quad (168)$$

in which $r' = r - r_i$, where r is the observation point, and $K_0[J]$ is the modified Bessel function of the second kind of order zero. The matrix equivalent form of Equation (167) is

$$[H]\{\Phi\} = [G]\{q\} + \{B\} \quad (169)$$

where $[H]$ and $[G]$ are banded sparse matrices, Φ , q , and B are vectors composed of nodal potentials ϕ , centroidal q_n and discretized domain integrals, respectively.

7.7 Lagrangian Particle Technique

Particle positions are calculated to simulate mass transport from both advection and diffusion. The transport equation can be written in the form

$$\frac{\partial C}{\partial t} + \frac{\partial U_i C}{\partial x_i} = 0 \quad (170)$$

where the velocity vector U_i is expressed in terms of advection and "flux" diffusion (Runchal, 1980)

$$U_i = \hat{U}_i + U_{f_i} \quad (171)$$

with U_i being the true advection velocity vector and the "flux" velocity defined as

$$U_{fi} = -\sum_j \frac{K_{ij}}{C} \frac{\partial C}{\partial x_j} \quad (172)$$

By combining the advection and diffusion terms together, a total equivalent transport velocity can be obtained. The form of the transport equation becomes identical to the equation of continuity for a general compressible fluid. The original problem of turbulent diffusion is transformed into one describing the advective changes of fluid density in a compressible fluid moving in a velocity field of total equivalent transport velocities. Mass particles are synonymous with density and follow the fluid motion in the velocity field, i.e., they are Lagrangian particles in a non-solenoidal field of total equivalent transport velocity. Their number in any location (volume) determines the concentration of pollutant for the original diffusion problem.

The probability distribution function for a three-dimensional space is (Runchal, 1980)

$$P_{x_i}(x_i, t) = \frac{1}{(4\pi t)^{\frac{3}{4}} (K_1 K_2 K_3)^{\frac{1}{2}}} \exp\left\{-\sum_{i=1}^3 \frac{(x_i - U_i t)^2}{4K_{it}}\right\} \quad (173)$$

where x_i are the position vectors in the direction of the principal axes and $K_1 K_2 K_3$ are the diagonal components of the second-order dispersion tensor in the direction of the principal axes.

The transport equation for this distribution can be written as $P=P(x_i, t)$

$$\frac{\partial P}{\partial t} + \frac{\partial}{\partial x_i} (U_i P) = \frac{\partial}{\partial x_i} (K_{ij} \frac{\partial P}{\partial x_j}) \quad (174)$$

where the tensor summation convention has been employed and K_{ij} is a second-order dispersion tensor. The inclusion of particle decay, settling, and more complex dispersion processes involving specified turbulence correlations, and can be included in Equation (174).

The problem of transport of particles by advection and dispersion commonly represented by a deterministic transport equation such as Equation (174) can also be represented simply as a series of random walks. Each of these random walks is composed of a deterministic advection component and a random component.

For example, the increment in the position vector of a particle at any time t can be written as

$$x_t - x_o = \int_{t_o}^t U(x_{t'}, t') d't' + \int_{t_o}^t D(x_{t'}, t') dw_{t'} \quad (175)$$

where D is a deterministic forcing function for the random component of motion. Equation (175) can be expressed simply as

$$\delta x(w, t) = \delta x_U + \delta x_D \quad (176)$$

with

$$\delta x_D(w, t) = \int_{t_o}^t n_r \sqrt{2K} d't' \quad (177)$$

where D is assumed equivalent to K and n_r is a normally distributed random number with a mean value of zero, and a standard deviation of unity. The integral Equation (174) can be further simplified to

$$\begin{aligned} \delta x_D &= n_r \sigma \\ \sigma^2 &= \int_{t_o}^t 2K d't' \end{aligned} \quad (178)$$

The variance obtained from Equation (175) is the same as that from Equation (174). Thus, Equation (172) can be written as

$$x_t - x_o = \int_{t_o}^t U(x_{t'}, t') d't' + n_r \left\{ \int_{t_o}^t (2K(x_{t'}, t') d't' \right\}^{1/2} \quad (179)$$

For a rigorous application of the random walk method, the net particle displacement must be calculated by integration of Equation (179). However, with U and K as arbitrary functions of space and time, it is not always possible to obtain a closed form solution. It is generally sufficient to assume that the mean velocity and random components can be separately calculated and linearly superimposed.

For steady or quasi-steady flows, the time scale of particle motion is much smaller than the characteristic time scale of change in the mean velocity and the dispersion fields. In such a case, it is often more convenient to express U and K as functions of the position vector x_i , rather than as Lagrangian functions of time.

In the application of the random walk model, the particle displacement in each of the coordinate directions is independently calculated from the displacement algorithm, Equation (179). Before this is performed, however, the mean velocity, U , and the dispersion due to turbulence or other stochastic mechanisms must be specified. The velocity of any particle is obtained from the application of the BEM, which can be used to obtain velocity components anywhere within the problem domain without the need for a nodal mesh or interpolation. A general

probability distribution or correlation function for the random component of motion due to dispersion is utilized to account for the dispersivity tensor, K .

The calculation to advance the particle configuration in time proceeds in steps, or cycles, each of which calculates the desired quantities for time $t + \Delta t$ in terms of those at time t . Hence,

$$x_i(t + \Delta t) = x_i(t) + U_i \Delta t \quad (180)$$

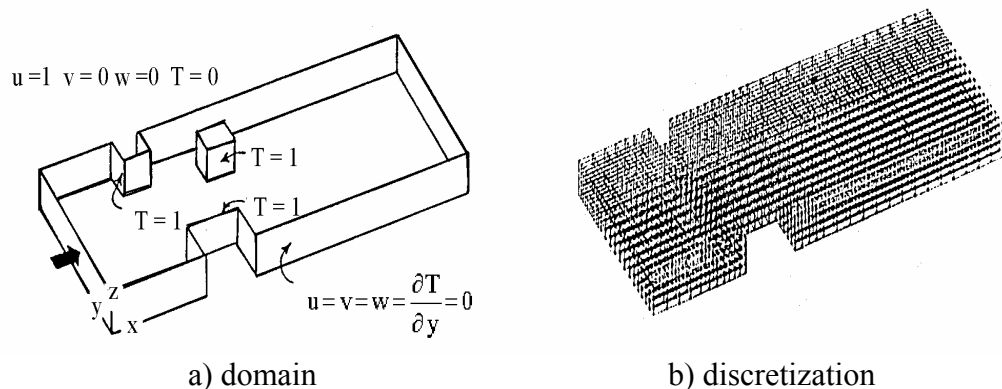
The velocity components are the fictitious total velocities determined for the beginning of the time interval and initial particle positions. Every particle is advanced in each cycle to a new position using Equation (180). Thus, the particle traces out in time a trajectory for the pollutant mass. Boundary conditions are introduced by modifications of the fictitious total velocities. Solid boundaries are simulated by not allowing particles to be transported across the boundaries. In each cycle, the fictitious total velocity for each cell is calculated as the sum of the advection velocity and the random turbulent flux velocity. The particle positions are updated using an interpolated total velocity. The concentration per unit volume is calculated from the particle masses.

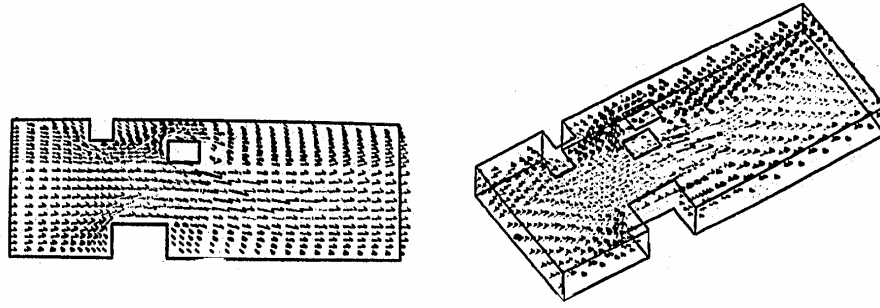
7.8 CFD Examples

Example 1: 3-D Airflow Around Heated Obstacles

For this problem, 3-D airflow is calculated around a set of heated obstacles. The physical domain and mesh are shown in Fig. 15 (a,b). The mesh consists of 2868 hexahedral elements; the Reynolds number is $Re = 10^3$ and $Pr = 1.0$. This type of problem commonly occurs in HVAC where obstructions are encountered within the flow domain.

Figure 15 (c,d) gives normal and perspective views of the 3-D velocity vectors within the channel. Recirculation of the flow occurs behind the blocks and small secondary cells develop in the corners. Thermal plumes emanate from the heated blocks; plume impingement from the left forward block occurs on the small mid-stream block. It is well known that when flow separates at the corners of blocks, horseshoe-like vortices are generated (Hunt et al., 1978).



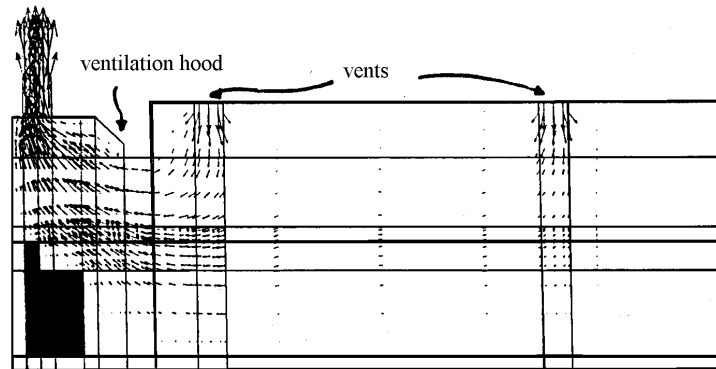


c) plane view of velocity vectors d) 3-D view of velocity vectors

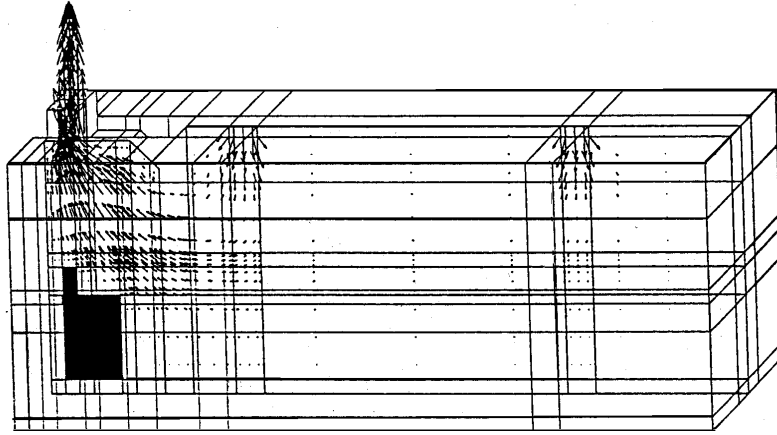
Figure 15. Airflow around heated obstacles.

Example 2: Air Flow over a Heated Oven within a Commercial Kitchen

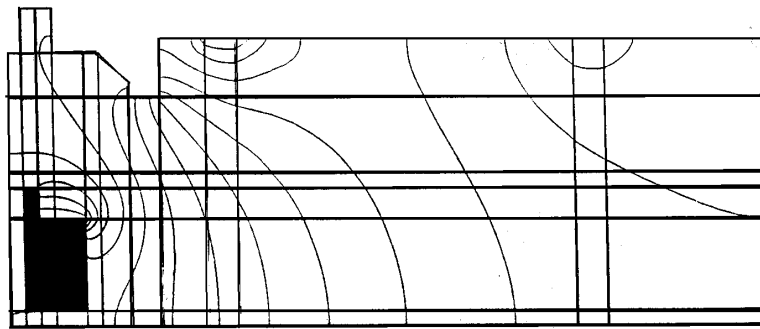
In this simulation, air enters the kitchen from two ceiling vents (and entrainment from the right open boundary), passes over the heated surface of the oven, and exits through the upper left corner of the exhaust hood as shown in Figure 16 (a-c). The heated surface acts to enhance the air motion, eventually accelerating the room air out the domain, and illustrates the ability of the spectral-element method to accommodate mixed convection problems (where the flow transitions from motion due strictly to natural convection to strongly forced convection).



a) velocity vectors in side view of kitchen



b) velocity vectors in 3-D view of kitchen

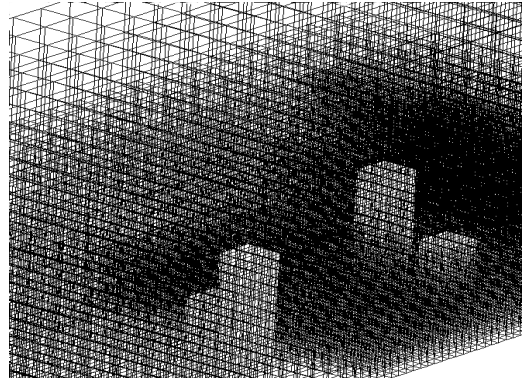


c) isotherms

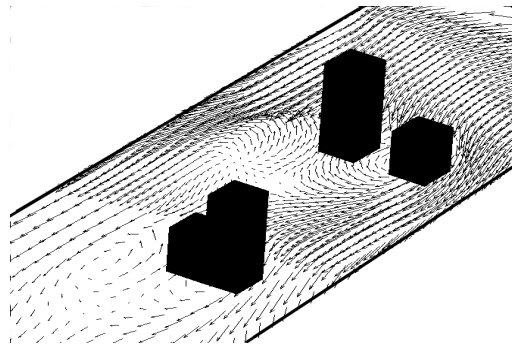
Figure 16. Flow over a heated oven in a commercial kitchen.

Example 3: 3-D Particulate Transport over Barriers

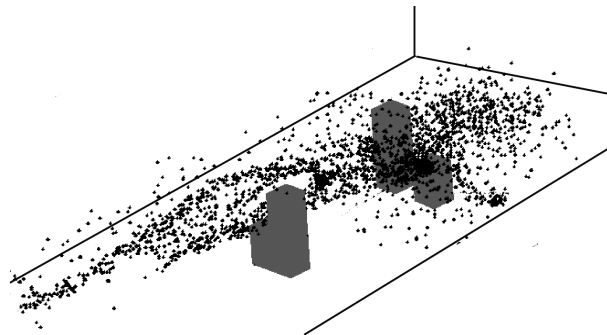
This example problem is modeled as a three-dimensional isothermal flow with a contaminant source located in front of the barriers. In this problem, the physical domain contains different size barriers. Three-dimensional hexahedrals are used to model the domain as shown in Figure 17 (a-c). The Petrov-Galerkin technique is used to eliminate numerical oscillations since there is a strong advection component to the problem. In this instance, the finite element method is used to establish the problem domain.



a) h-adapted finite element mesh



b) velocity vectors in horizontal plane



c) Lagrangian particles released into flow

Figure 17. 3-D particulate flow over a set of barriers.

A three-dimensional simulation of the airflow within the room is first calculated; mid-level velocity streak lines are shown in Figure 17 (b). A continuous source is released and the trajectory of the plume is illustrated using Lagrangian particles. In this simulation, two different particle sizes (light and heavy) are used, and the particles are advected and diffused in 3-D (Figure 17 c). Notice the plume of the light particles as they begin to disperse over the lower of the two barriers. The heavy particles eventually settle to the floor behind the first barriers. The simulations replicate the dispersion, and clearly show the spread of contaminant (e.g., smoke, based on particulate size).

Example 4: BEM-LPT model of particle dispersion

Figure 18 (a-c) shows the flow of air and particulate paths within a vented room. An [animation](#) is provided in the CD-ROM version of the book. Particles are released from a source located on the floor of the room. When the door on the right side of the room is opened, the plume bends towards the door, and begins to flow towards the lower pressure. The dispersion pattern of the particulates is more widely spread when the door is open – this is due primarily to the size of the opening.

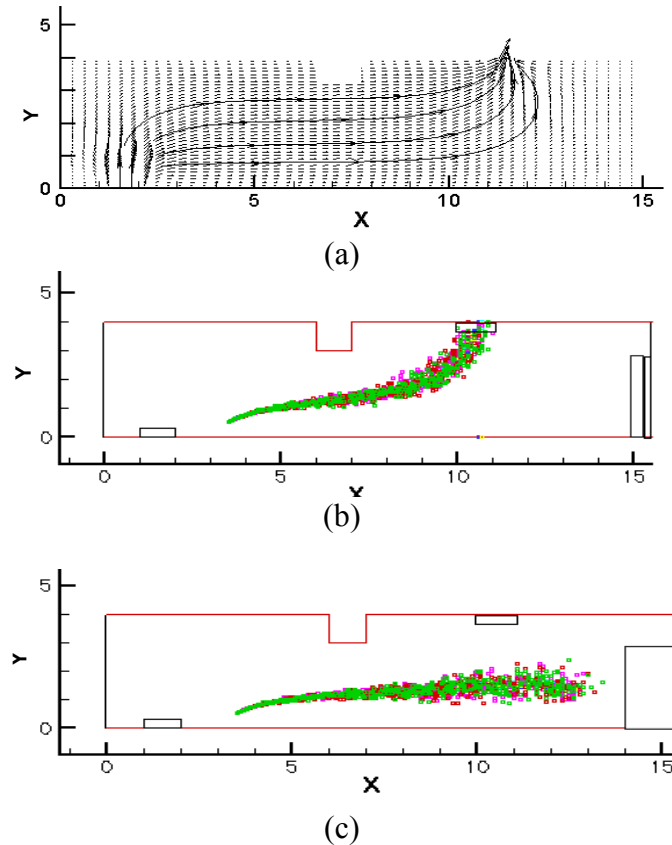


Figure 18. Indoor flow and particulate dispersion (a) velocities and streamlines, (b) door closed, and (c) door opened. An [animation](#) is provided in the CD-ROM version of the book.

7.9 Model Verification and Validation

A great deal of work has been done on verifying and validating results obtained with numerical models. Such efforts include comparing results between numerical and analytical models, sensitivity analyses, and seeing how well the numerical model predicts actual results obtained from experimental data. This latter comparison can be fairly tricky if some of the parameters, e.g., exchange coefficients, are not known in the actual experiment. A detailed discussion on model verification and validation can be found in the text by Roache (1998).

Efforts involved in validating and verifying numerical results with experimental data are not trivial - evaluations and comparisons must be carefully considered. These techniques include measures of difference, Pearson, Spearman, and Kendall correlations, skewness and kurtosis, tests for normality, and scatter diagrams (Pepper, 1981). These analyses help to provide insight into the physics of indoor air quality, and enable relations to be constructed to more reliably predict exposures.

References

- Anderson, D.A, Tannehill, J.C, and Pletcher, R.H., *Computational Fluid Mechanics and Heat Transfer*, Hemisphere, Wash., DC, 1984.
- American Society of Heating, Refrigerating and Air-Conditioning Engineers, *ASHRAE Handbook 1981 Fundamentals Volume*, Chpt. 22, Atlanta, GA, 1981, pp. 22.1-22.20
- Ames, B. N., Magaw, R., and Gold, L. S., "Ranking Possible Carcinogenic Hazards," *Science*, 236, 17 April 1987, pp. 271-280.
- Awbi, H. B., "Application of Computational Fluid Dynamics in Room Ventilation," *Build. Environ.*, 24, 1989, pp. 73-84.
- Awbi, H. B., *Ventilation of Buildings*, Chapman and Hall, London, 1991.
- Brain, J. D. and Beck, B. D., "Bioassays for Mineral Dusts and Other Particulates, *In Vitro Effects of Mineral Dusts*, E. B. Beck and J. Bignon (Eds.), NATO ASI Series Vol. G3, Springer Verlag, Berlin, 1985, pp. 323-335.
- Brebbia, C. A. and Dominguez, J., *Boundary Elements, An Introductory Course*, Comp. Mech. Pub., Southampton, U.K., 1989.
- Carrington, D. B., "Finite Elements with h-adaptation for Momentum, Heat, and Mass Transport with Application to Environmental Flow," Ph.D. Dissertation, University of Nevada - Las Vegas, Department of Mechanical Engineering, Las Vegas, NV, 2000.
- Carslaw, H. S. and Jaeger, J. C., *Conduction of Heat in Solids*, Oxford University Press, London, UK, 1947.
- Cooper, D. C., Alley, F. C., *Air Pollution Control A Design Approach*, 2nd edition, Prospect Heights, Illinois, Waveland Press, Inc., 1994.
- Davidson, L., "Numerical Simulation of Turbulent Flow in Ventilated Rooms," PhD. Thesis, Chalmers Univ. of Tech., Gotenborg, 1989.
- Davies, C. N., *Chapter XII Deposition from Moving Aerosols*, C. N. Davies (Ed.), *Aerosol Science*, NY, NY, Academic Press, 1966, pp. 409-428.
- Deardorff, J. W., "A Numerical Study of Three-Dimensional Channel Flow at Large Reynolds Numbers," *J. Fluid Mech.*, 41, 1970, pp. 453-480.
- Eguchi, Y., Yagawa, G., and Fuchs, L., "A Conjugate-Residual-FEM for Incompressible Viscous Flow Analysis," *Comp. Mech.*, Vol. 3, No. 1, 1988, pp. 59-72.

Fletcher, C.A.J., "Computational Techniques for Fluid Dynamics - Volume II," 2nd ed., Springer-Verlag, NY, 1991, pp. 47-78.

Fuchs, N. A., *The Mechanics of Aerosols*, Pergamon Press, NY, 1964.

Gosman, A. D., Pun, W. M., Runchal, A. K., Spalding, D. B., and Wolfshtein, M., *Heat and Mass Transfer in Recirculating Flows*, Academic Press, London, 1969.

Gosman, A. D., Nielsen, P. V., Restivo, A., and Whitelaw, J. H., "The Flow Properties of Rooms with Small Ventilation Openings," *Trans. ASME, J. Fluid Engr.*, 102, 1980, pp. 316-323.

Gresho, P. M., Chan, S. T., Lee, R. L., and Upson, C. D., "Modified Finite Element Method for Solving the Time-Dependent Incompressible Navier-Stokes Equations, Part 1, Theory," *Int. J. Num. Meth. Fluids*, 4, 1984, pp. 557-598.

Hansen, G. A., "Scalability of Preconditioners as a Strategy for Parallel Computation of Compressible Fluid Flow," Ph.D. Dissertation, University of Idaho, Department of Computer Science, Idaho Falls, ID, 1996.

Harlow, F. H. and Welch, J. E., "Numerical Calculation of Time-Dependent Viscous Incompressible Flow of Fluid with Free Surfaces," *Phys. Fluids*, 8, 1965, pp. 2182-2189.

Hayes, S. M., Gobbell, R. V., and Ganick, N. R., *Indoor Air Quality: Solutions and Strategies*, McGraw-Hill, Inc., NY, 1995.

Heinsohn, R. J., *Industrial Ventilation: Engineering Principles*, J. Wiley & Sons, NY, 1991.

Hjertager, B. H. and Magnussen, B. F., "Numerical Prediction of Three-Dimensional Turbulent Buoyant Flow in a Ventilated Room," *Heat Transfer and Turbulent Buoyant Convection*, D. B. Spalding and N. Afgan (Eds.), Vol. II, Hemisphere, Washington, DC, 1977, pp. 429-441.

Hunt, J.C., Abell, C.J., Peterka, J.A., and Woo, H., "Kinematical Studies of the Flows around Free or Surface Mounted Obstacles; Applying Topology to Flow Visualization," *J. Fluid Mech.*, 86, 1, 1978, pp.179-200.

Hinds, W.C., *Aerosol Technology – Properties, Behavior, and Measurement of Airborne Particles*, J. Wiley & Sons, NY, Inc., 1982, pp. 155-156.

Jones, W. P. and Launder, B. E., "The Prediction of Laminarization with a Two-Equation Model of Turbulence," *Int. J. Heat Mass Transfer*, 15, 1972, pp. 301-314.

Markatos, M. C. and Cox, G., "Hydrodynamics and Heat Transfer in Enclosures Containing a Fire Source," *Phys. Chem. Hydrodyn.*, 5, 1984, pp. 53-66.

Martin, R.A., Tang, P.K., Harper, A.P., Novat, J.D., and Gregory, W.S., *Material Transport Analysis for Accident-Induced Flow in Nuclear Facilities*, NUREG/CR-3527, Los Alamos, NM, Los Alamos National Laboratory, 1983.

Moult, A. and Dean, R. B., "CAFE-A Computer Program to Calculate the Flow Environment," CAD 80, *4th Int. Conf. on Computers in Design Engineering*, Brighton, UK, 1980.

Murakami, S., Tanaka, T., and Kato, S., "Numerical Simulation of Air Flow and Gas Diffusion in Room Model - Correspondence between Numerical Simulation and Model Experiment," *Proc. 4th CIB Int. Symp. on the Use of Computers for Environmental Engineering Related to Buildings*, Tokyo, 1983, pp. 90-95.

Murakami, S., Kato, S., and Suyama, Y., "Three-Dimensional Numerical Simulation of Turbulent Airflow in a Ventilated Room by Means of a Two-Equation Model," *ASHRAE Trans.*, 93(2), 1987, pp. 621-642.

Nielsen, P. V., "Flow in Air Conditioned Rooms," PhD Thesis, Tech. Univ. of Denmark, 1974.

Nielsen, P. V., "Contamination Distribution in Industrial Areas with Forced Ventilation and Two Dimensional Flow," *Int. Inst. of Refrigeration, Joint Meeting E1*, Essen, W. Germany, 1981, pp. 223-230.

Pasquill, F. and Smith, F. B., *Atmospheric Diffusion*, 3rd Ed., Ellis Horwood Ltd., Chichester, UK, 1985.

Patankar, S. V. and Spalding, D. B., "A Calculation Procedure for Heat, Mass, and Momentum Transfer in Three-Dimensional Parabolic Flows," *Int. J. Heat Mass Transfer*, 15, 1972, pp. 147-163.

Patankar, S. V., *Numerical Heat Transfer and Fluid Flow*, Hemisphere, NY, 1980.

Pelletier, D. and Ilinca, F., "An Adaptive Finite Element Method for Mixed Convection Heat Transfer," presented at the 32nd AIAA Aerospace Sci. Meeting, Jan. 10-13, 1994, Reno, NV, paper AIAA-94-0347

Pepper, D. W., "Modeling of Three-Dimensional Natural Convection with a Time-Split Finite Element Technique," *Num. Heat Transfer*, Vol. 11, 1987, pp. 31-55.

Pepper, D. W. and Singer, A. P., "A Modified Finite Element Method for the Personal Computer," *Num. Heat Transfer*, Vol. 11, 1990, pp. 31-55.

Pepper, D. W. and Emery, A. F., "Atmospheric Transport Prediction using an Adaptive Finite Element Method," *Proc. 5th Int. High Level Rad. Waste Manag. Conf.*, 1994, pp. 1946-1952.

Pepper, D. W., "Results from the Savannah River Laboratory Model Validation Workshop, Nov. 19-21, 1980," *Proceedings of the 5th Symp. on Turbulence, Diffusion, and Air Pollution*, March 9-13, 1981, Atlanta, GA.

Pozrikidis, C. (1999), *Little Book of Streamlines*, Academic Press, San Diego, CA.

Pruppacher, H. R. and Klett, J. D., *Microphysics of Clouds and Precipitation*, D. Reidel Pub. Co., Dordrecht, Holland, 1978.

Reist, P.C., *Aerosol Science and Technology*, 2nd Ed., McGraw-Hill, Inc., NY, 1993.

Repace, J. L. and Lowery, A. H., "Indoor Air Pollution, Tobacco Smoke, and Public Health," *Science*, 208, May 1980, pp. 464-472.

Roache, P. J., *Verification and Validation in Computational Science and Engineering*, Hermosa Pub., Albuquerque, NM, 1998.

Runchal, A. K., "A Random Walk Atmospheric Dispersion Model for Complex Terrain and Meteorological Conditions," *2nd AMS Joint Conf. on Appl. of Air Pollution Meteor.*, March 24-27, 1980, New Orleans, LA.

Sakamoto, Y. and Matsuo, Y., "Numerical Predictions of Three-Dimensional Flow in a Ventilated Room using Turbulence Models," *Appl. Math. Modelling*, Vol. 4, 1980, pp. 67-71.

Thompson, J. F., Warsi, Z. U. A., and Martin, C. W., *Numerical Grid Generation*, North-Holland, NY, 1985.

Vargaftik, N. B., *Tables on the Thermophysical Properties of Liquids and Gases*, 2nd Ed., Hemisphere Pub. Corp., Washington, DC, 1975.

Woo, T-C. and Hwang, C. C., *Classic Analytical Problems in Mechanical Engineering*, R. T. Edwards, Inc., Flouertown, PA, 2000..

Yu, C.C. and Heinrich, J.C., "Petrov-Galerkin Methods for the Time-Dependent Convective Transport Equation," *Int. J. Num. Methods in Engr.*, Vol. 23, 1986, p. 883-890.

Zienkiewicz, O.C., *The Finite Element Method*, McGraw Hill, London, 1977.